AD-A039 988 DELAWARE UNIV NEWARK DEPT OF CIVIL ENGINEERING F/G 8/3
MEASUREMENTS AND COMPUTATION OF WAVE SPECTRAL TRANSFORMATION AT--ETC(U)
NOV 76 H WANG, W YANG N00014-76-C-0342
UNCLASSIFIED OCEAN ENGINEERING-11 NL

1 OF 2
AD A039988

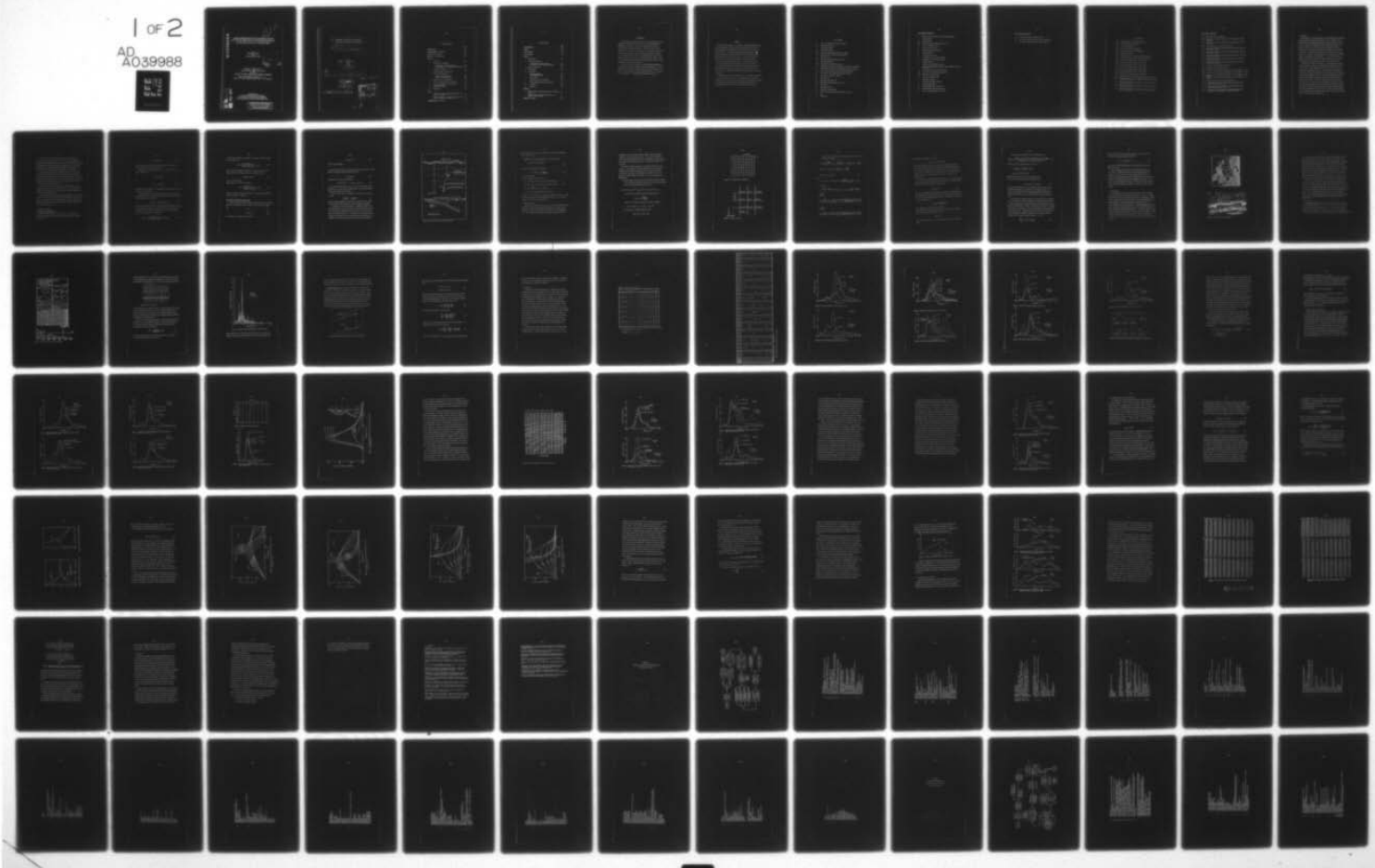

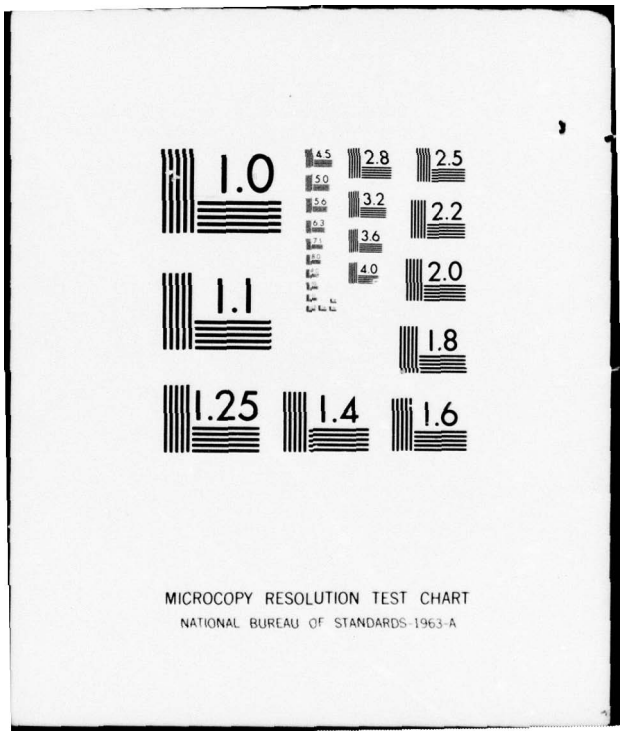
1.0
1.1
1.25
1.4
1.6
1.8
2.0
2.2
2.5
2.8
3.2
3.6
4.0
4.5
5.0
5.6
6.3
MICROCOPY RESOLUTION TEST CHART
NATIONAL BUREAU OF STANDARDS-1963-A

MEASUREMENTS AND COMPUTATION OF WAVE SPECTRAL TRANSFORMATION AT ISLAND OF SYLT, NORTH SEA

by
HSIANG WANG
and
WEI-CHONG YANG

TECHNICAL REPORT NO. 3
Contract No. N0014-76-C-0342
with the
OFFICE OF NAVAL RESEARCH GEOGRAPHY PROGRAMS

OCEAN ENGINEERING REPORT NO. 11
Dept. of Civil Engineering, Univ. of Delaware

Sonderdruck
aus Heft 52 (1976) der Mitteilungen
des Leichtweiss-Instituts für Wasserbau
der Technischen Universität Braunschweig

(6) MEASUREMENTS AND COMPUTATION OF WAVE SPECTRAL TRANSFORMATION AT ISLAND OF SYLT, NORTH SEA

(9) Technical rept.

BY

(10) Hsiang Wang

[redacted]

Wei-Chong Yang

(14) Ocean Engineering-11, TR-3

401 595

(11) Nov[redacted]76

(12) 104p.

(15) N00014-76-C-0342

6pg

INHALTSVERZEICHNIS

		Seite
VORBEMERKUNGEN		198
ZUSAMMENFASSUNG (in Englisch)		199
VERZEICHNIS DER SYMBOLE		200
VERZEICHNIS DER ABBILDUNGEN		203
ABSCHNITT		
1	Einleitung	205
2	Theoretische Grundlagen	
	Veränderungen von Wellenspektren	206
	Wellenkennwert k und Energie-Transformation	208
3	Numerische Verfahren	211
4	Durchführung der Naturmessungen	217
5	Auswertung der Meßdaten	
	Spektren der Wellenenergie	219
	Winkel der Wellenfronten	223
6	Ergebnisse der Naturmessungen	225
7	Numerische Ergebnisse und Vergleiche	233
8	Gleichgewichtsbereich für Wellen in begrenzter Wassertiefe	245
9	Schlußfolgerungen	263
10	Schrifttum	266
ANHANG		
1	Computer Programm - Schwingungserzeugung und Analyse der Spektren	268
2	Computer Programm - Veränderungen des Spektrums über unregelmäßigen Sohlenformationen	285
ZUSAMMENFASSUNG (in Deutsch)		299

TABLE OF CONTENTS

		Page
ACKNOWLEDGEMENTS		198
SUMMARY		199
LIST OF SYMBOLS		200
LIST OF FIGURES		203
CHAPTER		
1	Introduction	205
2	Theoretical Background	
	Transformation of Energy Spectrum	206
	Wave Number and Wave Energy Transformation	208
3	Numerical Procedures	211
4	Field Program	217
5	Data Analysis	
	Wave Energy Spectra	219
	Wave Approaching Angles	223
6	Field Results	225
7	Numerical Results and Comparisons	233
8	Equilibrium Range in Wave of Finite Depth	245
9	Conclusions	263
10	References	266
APPENDICES		
1	Computer Program - Periodogram Generator and Spectral Analysis	268
2	Computer Program - Spectral Transformation Over Irregular Bottom Topography	285
SUMMARY (in German)		299

ACKNOWLEDGMENT

The authors wish to express their sincere thanks to Professor Dr. Alfred Führböter, Leichtweiß-Institut für Wasserbau der TECHNISCHEN UNIVERSITÄT BRAUNSCHWEIG, West Germany. Without his encouragement and consent the field work would not have been carried out. They also owe their special thanks to Dr. H. H. Dette of the same Institute, who provided and organized the field party and consistently lent his helping hand throughout the project. Mr. E. Martini who led the field group has performed the duty at the highest standard to bring the project to its successful conclusion. Thanks are also due to Mr. Hollmann in constructing the field apparatus and to Messrs. Zitscher and Waschko who performed the field work.

This work was jointly sponsored by the DEUTSCHE FORSCHUNGS-GEMEINSCHAFT (German Research Foundation), BRANDUNGSSTAU UND BRANDUNGSENERGIE - FU 96/10 and the Office of Naval Research, Geography Programs Contract No. N0014-76-C-0342 while the senior author was visiting the Technical University of Braunschweig partially sponsored by the MINNA-JAMES-HEINEMAN-STIFTUNG of Hannover.

SUMMARY

Wave spectra were measured in the nearshore region extending approximately 900 m from the shore at the Island of Sylt (North Germany) in the North Sea. Seven gage stations were in operation for a period of two weeks in May, 1976 for data collection. The field results were presented and compared with numerical computations for energy transformation in shallow water, based on a method developed earlier for the same project. The numerical computation agreed well with the field data in the range of energy-containing wave components and low frequency components but failed in high frequency range.

Based upon commonly-used wave instability criteria, an equilibrium energy spectral density function in water of finite depth has been developed. This function provides saturation conditions on spectral density for the complete spectrum. Comparison with field data is encouraging but, nevertheless, inconclusive.

Combining field evidence and numerical results, an assessment has been made on the wave climate of the test area. It was demonstrated that the offshore bar located in the test area plays a double role as energy dissipator and trapper. It was also shown that waves from the N-W quadrant are more effective in generating longshore current and thus in longshore material transport.

LIST OF SYMBOLS

A_o	Tidal level measured from mean water level (M)
A_c	Limiting wave amplitude
C	Wave celerity (m/sec)
C_g	Group velocity (m/sec)
$\overline{C}_{ij}$	Mean wave celerity between gages i and j (m/sec)
DF	Degree of freedom in spectral density analysis
d	Water depth (M)
$\overline{d_{ij}}$	Mean water depth between gages i and j (M)
E	Wave total energy (M^2)
$F(\vec{k})$	Wave number spectral density function
Ga	Normalized wave frequency equilibrium function based on acceleration
Gu	Normalized wave frequency equilibrium function based on velocity
g_a	Wave frequency equilibrium function based on acceleration
g_u	Wave frequency equilibrium function based on velocity
g	Gravitational acceleration (m/sec^2)
H	Wave height (M)
H_s	Significant wave height (M)
$\overline{H}_{ij}$	Mean wave height between gages i and j (M)
k	Wave number
$\vec{k}$	Wave number in vector
L_s	Significant wave length (M)
ℓ	Depth of transducer measured from mean water level (M)
M	Meter
m	Bottom slope

List of Symbols (Continued)

N	Number of real data points in spectral density analysis
n	Wave frequency
$S_{\alpha\beta}$	Radiation stress
S_{ij}	Horizontal distance between gages i and j (M)
S_i	Station i (Defined in Fig. 5)
S	Spectral density (m^2-sec)
Sp	Pressure spectral density (m^2-sec)
U	Wind speed (m/sec)
$\vec{u}$	Current velocity (m/sec)
u	x-component of current velocity (m/sec)
v	y-component of current velocity (m/sec)
α	Phillips constant
β	Constant in Poison-Moskowitz spectrum
ν	The ratio of maximum spectral density between JONSWAP spectrum and P-M spectrum
Δt	Time interval in spectral density analysis
Δt_{ij}	Time of wave front traveling from gage i to j
Δx	Grid size in x-direction (M)
Δy	Grid size in y-direction (M)
σ	Wave angular frequency
σ_o	Deep water wave angular frequency
θ	Wave approaching angle
θ_o	Wave approaching angle in deep water
θ_m	Maximum expected wave approaching angle
ϵ	Rate of energy dissipation per unit area

List of Symbols (Continued)

$\phi_{(n)}$	Wave frequency spectral density function
ϕ_a	Wave number equilibrium function based on acceleration
ϕ_u	Wave number equilibrium function based on velocity

LIST OF FIGURES

Fig. 1 Definition sketch of nearshore environment

Fig. 2 Grid system used in computation
F
Fig. 3 Local grid description

Fig. 4 Site location and area hydrograph

Fig. 5 Gage locations and nearshore hydrograph

Fig. 6 Sample of wave data

Fig. 7 Comparison between periodogram and smoothed spectrum

Fig. 8 Shallow water gage arrays for directional information

Fig. 9 Wave spectra measured on May 3, 1976 at 15:45

Fig. 10 Wave spectra measured on May 5, 1976 at 11:00

Fig. 11 Wave spectra measured on May 5, 1976 at 16:15

Fig. 12 Wave spectra measured on May 6, 1976 at 14:50

Fig. 13 Wave spectra measured on May 7, 1976 at 18:00

Fig. 14 Wave spectra measured on May 11, 1976 at 10:15

Fig. 15 Wave spectra measured on May 11, 1976 at 16:20

Fig. 16 Estimated wave and swell approaching angles and wind directions

Fig. 17 Comparison among field data, JONSWAP and P-M spectra (Data from May 3, 1976 at 15:45)

Fig. 18 Comparison among field data JONSWAP and P-M spectra (Data from May 5, 1976 at 11:00)

Fig. 19 Comparison among field data JONSWAP and P-M spectra (Data from May 11, 1976 at 10:15)

Fig. 20 Comparison among field data JONSWAP and P-M spectra (Data from May 11, 1976 at 16:20)

List of Figures (Continued)

Fig. 21 Hypothetical rhythmic topography

Fig. 22 Illustrations of spectral variations of wave spectrum over rhythmic topography

Fig. 23 Illustrations of spectral variations of wave spectrum over an offshore ridge

Fig. 24 The bottom-depth chart used as numerical input

Fig. 25 Comparison of measured and computed shallow water spectra (Data from May 5, 1976 at 16:20)

Fig. 26 Comparison of measured and computed shallow water spectra (Data from May 6, 1976 at 14:50)

Fig. 27 Comparison of measured and computed shallow water spectra (Data from May 11, 1976 at 10:15)

Fig. 28 Comparison of measured and computed deep water spectra (Data from May 5, 1976 at 16:15)

Fig. 29 Comparison of measured and computed deep water spectra (Data from May 11, 1976 at 10:15)

Fig. 30 Variation of k^3 Ga(k) and k^3Gu(k) with kd

Fig. 31 Variation of Ga(k) and Gu(k) with kd

Fig. 32 Variation of $\phi_a(n)$ and $\phi_u(n)$ with respect to u for a constant d = 1.5 M

Fig. 33 Variation of $\phi_a(n)$ and $\phi_u(n)$ with respect to u for a constant d = 3.0 M

Fig. 34 Variation of $\phi_a(n)$ and $\phi_u(n)$ with respect to d for a constant u = -0.5 M/sec

Fig. 35 Variation of $\phi_a(n)$ and $\phi_u(n)$ with respect to d for a constant u = -1.0 M/sec

Fig. 36 Composite equilibrium curve of breaking criteria

Fig. 37 Comparisons between field data and composite equilibrium curves (Data from May 3 and May 7, 1976)

Fig. 38 Comparisons between field data and composite equilibrium curves (Data from May 5 and May 11, 1976)

Fig. 39 Comparison of spatial variations of near-breaking wave angles approaching from N-W quadrant to that from S-W quadrant

1. Introduction

The utilization of wave energy spectrum as a statistical measure to describe the ever-irregular ocean wave has become, more or less, a standard practice. Armed with this tool, oceanographic scientists have made significant progress in the past two decades in the development of wave forecasting techniques. The endeavor has been, however, mainly concentrated on deepwater situations. Consequently, the deep water wave climate can be assessed with certain degrees of confidence. To establish the wave climate in the coastal zone as is often necessary for scientific and engineering purposes the deepwater wave environment needs to be transformed into shoaling waters. It is in this area that both knowledge and effort are conspicuously lacking, although, odd as it may seem, the transformation of monochromatic wave train is a well studied topic.

At present, there exists a few attempts in the development of theoretical concepts and numerical techniques concerning spectral transformation from deep to shallow water. Longuet-Higgins (1956) and Collins (1972), for instance, have studied the theoretical formulation on wave spectrum by considering the conservation of energy between adjacent wave rays much the same way of the wave refraction in monochromatic wave trains. Based on Longuet-Higgins' formulation, Karlesson (1969) developed a method to compute spectrum transformation over parallel bottom contours. Collins (1972) extended the work to the inclusion of bottom friction. Krasitkiy (1974) has derived explicit analytical solutions for the spectrum transformation over two-dimensional parallel bottom contours More recently, Shiau and Wang (1976) developed a numerical technique to compute the spatial transformation of wave spectrum over irregular bottom topographies. Their work promises to be an effective method, though it has not been critically tested for lack of detailed field data as yet.

In May, 1976, a brief, but intensive, field work was carried out at the Island of Sylt (North Germany) in the North Sea to collect information on nearshore wave environment and beach process. One of the objectives was to better the understanding of nearshore wave energy transformation and to test validity and limitation on the numerical technique developed by Shiau and Wang. The material covered in this report deals specifically with this objective.

The field work covered a period of approximately two weeks. Wave spectra were measured at stations installed in water ranging from a 7-meter depth to less than 1 meter near the shoreline at low tide. During this period, the wave conditions were considered normal for this area with heights up to 1.5 to 2 meters. The winds varied in speed from as low as 3 m/s to more than 12 m/s; the wind directions covered both onshore and offshore.

These field results were compared with numerical predictions using the recorded offshore data as input. During the course of the study, the numerical procedure was further improved to relax the boundary condition requirements and to shorten the computational time.

An equilibrium spectral density function has been developed for the condition of water of finite depth. This function provides information on the saturation condition of energy density for the complete spectrum. Finally, combining field evidence and numerical results, an attempt was made to provide an assessment of the wave climate of the test area.

2. Theoretical Background

Transformation of Energy Spectrum

In its very general form, the total energy of a random seaway can be expressed as the summation of energy content in the wave number and frequency space such that

$$E = \int\int \chi(\vec{k},n)\, d\vec{k}\, dn \tag{1}$$

where E is the total energy; $\chi(\vec{k},n)$ is the spectral density function; $\vec{k}$ is the wave number and n is the wave frequency.

Reduced spectra can be obtained from $\chi(\vec{k},n)$ by integration over n and over $\vec{k}$. Thus, we have

$$F(\vec{k}) = \int_0^\infty \chi(\vec{k},n)\, dn \tag{2}$$

and

$$\phi(n) = \int \chi(\vec{k},n)\, d\vec{k} \tag{3}$$

where $F(\vec{k})$ and $\phi(n)$ are known as the wave number and wave frequency spectral density functions, respectively.

Since the wave number spectrum can be interpreted as a directional frequency spectrum owing to the dispersion relation between k and n, the following relationship exists (Phillips, 1966)

$$\phi(n,\theta)dn = [k\, F(k,\theta)\, dk]_{k = G(n)} \tag{4}$$

where k is the magnitude of $\vec{k}$ and θ is the direction of propagation and $k = G(n)$ is the dispersion relationship. Let subscript 0 denote the reference state (deepwater condition is usually conveniently selected), the transformation equation of frequency spectrum is established,

$$\phi(n,\theta)dn = \frac{[k\, F(k,\theta)dk]_{k = G(n)}}{\{[k\, F(k,\theta)dk]_{k = G(n)}\}_0} [\phi(n,\theta)\, dn]_0 \tag{5}$$

For steady state condition, the frequency n is invariant to space, the above equation simplifies to

$$\phi(n,\theta) = \frac{[k\ F(k,\theta)dk]_{k\ =\ G(n)}}{[k_o F_o(k,\theta)dk]_{k\ =\ G_o(n)}}\ \phi_o(n,\theta) \qquad (6)$$

Since $F(k,\theta)dk$ approximates the incremental of wave energy over the wave number band dk at a directional angle θ, it is plausible to write

$$F(k,\theta)dk = dE(k;\theta) \qquad (7)$$

with θ as a parameter here.

Substituting Eq. (7) into Eq. (6) results in

$$\phi(n,\theta) = \frac{[k\ dE(k;\theta)]_{k\ =\ G(n)}}{[k_o dE_o(k;\theta)]_{k\ =\ G_o(n)}}\ \phi_o(n,\theta) \qquad (8)$$

Therefore, to compute the spatial variations of ϕ, we must first establish the spatial variations of k and $dE(k;\theta)$.

Wave Number and Wave Energy Transformation

The basic equation to compute the spatial variations of k is the conservation equation for the wave number, which, for steady cases, reduces to the simple form

$$\nabla n = 0 \qquad (9)$$

or

$$n = \text{const} = \sigma_o \qquad (9\text{-}a)$$

In the presence of a steady current $\vec{u}$, we have

$$n = \sigma(k;d) + \vec{k} \cdot \vec{u} \tag{10}$$

where d is the water depth.

For regions where both d and $\vec{u}$ vary slowly over distances of the order of a wavelength, the following dispersion relationship exists,

$$\sigma^2 = gk \tanh kd \tag{11}$$

Combining Eqs. (9), (10) and (11) results in

$$(gk \tanh kd)^{1/2} + u\,k\cos\theta + v\,k\sin\theta = \sigma_o \tag{12}$$

for the coordinate system shown in Fig. I. Here u and v are current velocity components in the x and y directions respectively; θ is the wave approaching angle measured from the positive x-axis.

Since it is known that the wave-number vector in space is irrotational, it follows

$$\frac{\partial(k\cos\theta)}{\partial y} - \frac{\partial(k\sin\theta)}{\partial x} = 0 \tag{13}$$

For given spatial distribution of $\vec{u}$, Eqs. (12) and (13) enable us to compute k and θ in the wave region provided the boundary condition is specified.

To determine the variations of $dE(k;\theta)$, the assumption is made that the wave energy associated with a certain frequency band stays within this band so that the principal of energy conservation is applicable to each individual frequency band under consideration. This assumption denies energy transfer among different frequencies and is compatible only when nonlinear effects are negligible. Following the energy equation presented by Longuet-Higgins and

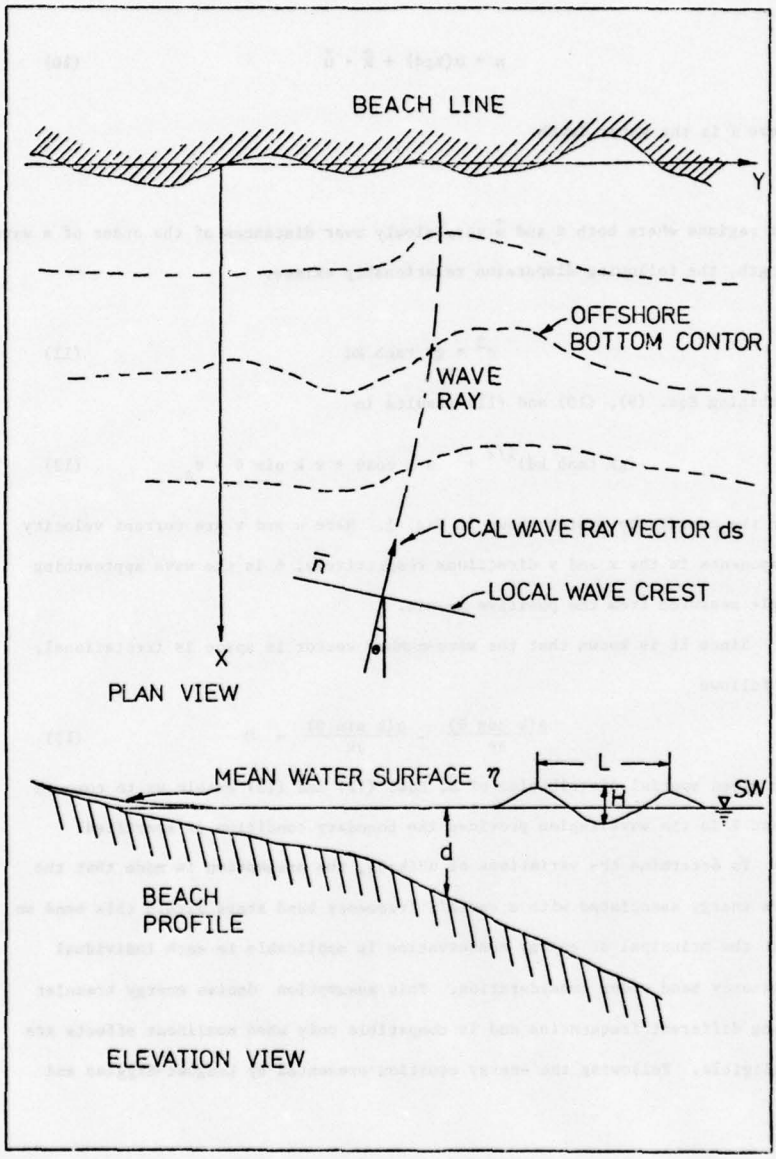

Fig. 1: Definition sketch of nearshore environment

Stewart (1960, 1961) for the fluctuating motion of waves with a superimposed current system, we have

$$\frac{\partial}{\partial x}\left[dE(k)(u + Cg\cos\theta)\right] + \frac{\partial}{\partial y}\left[dE(k)(v + Cg\sin\theta)\right] + S_{xx}\frac{\partial u}{\partial x} + S_{xy}\frac{\partial v}{\partial x} + S_{yy}\frac{\partial v}{\partial y} + S_{yx}\frac{\partial u}{\partial y} = -\Sigma \tag{14}$$

where Cg is the group velocity expressed as

$$n_g = \frac{Cg}{C} = \frac{1}{2}\left[1 + \frac{2kd}{\sinh(2kd)}\right] \tag{15}$$

C is the wave celerity

$S_{\alpha\beta}$ are the radiation stresses such that

$$\begin{aligned} S_{xx} &= dE(k)\left[(2n_g - \tfrac{1}{2})\cos^2\theta + (n_g - \tfrac{1}{2})\sin^2\theta\right] = dE(k)\,\sigma_{xx} \\ S_{yy} &= dE(k)\left[(2\,n_g - \tfrac{1}{2})\sin^2\theta + (n_g - \tfrac{1}{2})\cos^2\theta\right] = dE(k)\,\sigma_{yy} \\ S_{xy} &= S_{yx} = \frac{dE(k)}{2}\,n_g\sin(2\theta) = dE(k)\,\sigma_{xy} \end{aligned} \tag{16}$$

Σ is the rate of energy dissipation per unit area.

With known θ, Eq. (14) permits the computation of the spatial variations of dk(E) for given boundary conditions and the dissipation function. For the present computation, Σ is taken to be equal to zero.

3. Numerical Procedures

Based upon Eqs. (12), (13) and (14), Noda, et al. (1974) developed numerical procedures to compute the wave number and wave height as functions of space variables for beaches with periodical bottom variations in the longshore direction. Shiau and Wang (1976) extended the procedure to compute the spectrum

transformation with the boundary conditions somewhat relaxed to accommodate irregular but slowly varying bottom profiles. In the present computation, their method is further improved to relax the requirements of boundary conditions and to improve the computational efficiency. The procedures are briefly described here.

To facilitate numerical computation, the governing equations are, out of necessity, to be transformed into finite difference form. A mixed forward, backward and central differences scheme are used to minimize the boundary restrictions at the expense of nonuniformity of the order of errors. With reference to the grid schemes shown in Figs. 2 and 3 the key equations are summarized here:

(1) The wave number and wave angle are solved through numerical iterations of the wave-number conservation equation and the irrotational wave-number equation. The conservation equation [Eq. (12)],

$$[g\, k_{ij} \tanh (k_{ij}\, d_{ij})]^{1/2} + u_{ij}\, k_{ij} \cos \theta_{ij} + v_{ij}\, k_{ij} \sin \theta_{ij} = \sigma_o$$

is solved through a Newtonian iterative technique defined as:

$$k_{new} = k_{old} - \frac{f(k_{old})}{f'(k_{new})}$$

where f'(k) is the first derivative of f(k) which is defined:

$$f(k) = gk \tanh kh - [\sigma_o - uk \cos \theta - vk \sin \theta]^2$$

The iteration is considered satisfactory when

$$|k_{new} - k_{old}| \leq 0.001\, |k_{new}|$$

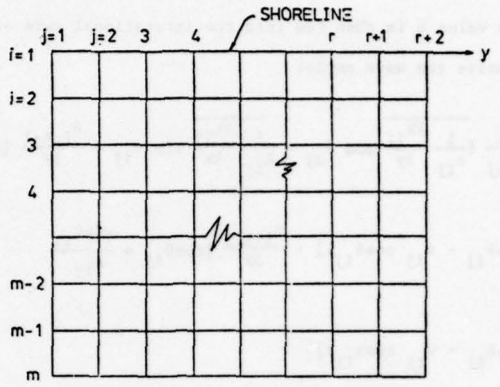

Fig. 2: Grid system used in computation

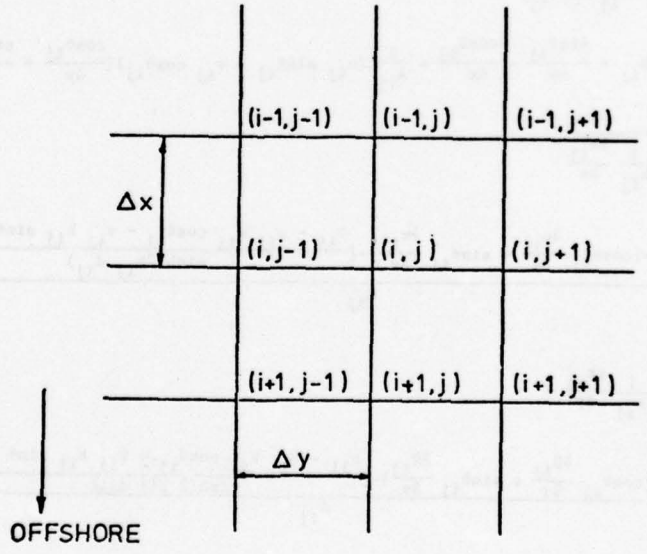

Fig. 3: Local grid description

This value k is then fed into the irrotational wave equation [Eq. (13)] to solve the wave angle:

$$\theta_{ij} = \frac{1}{B_{ij}} \{\overline{\frac{1}{k_{ij}} \frac{\partial k_{ij}}{\partial y}} \cos\theta_{ij} - \overline{\frac{1}{k_{ij}} \frac{\partial k_{ij}}{\partial x}} \sin\theta_{ij} + \frac{\theta_{i,j-1}}{\Delta y} [\sin\theta_{ij} - \frac{\cos\theta_{ij}}{A_{ij}} (u_{ij} \sin\theta_{ij} - v_{ij} \cos\theta_{ij})] - \frac{\theta_{i+1,j}}{\Delta x} [\cos\theta_{ij} + \frac{\sin\theta_{ij}}{A_{ij}} (u_{ij} \sin\theta_{ij} - v_{ij} \cos\theta_{ij})]\} \quad (17)$$

where

$$A_{ij} = u_{ij} \cos\theta_{ij} + v_{ij} \sin\theta_{ij} + \frac{1}{2} [1 + \frac{2k_{ij}d_{ij}}{\sinh(2 k_{ij}d_{ij})}][\frac{\sigma_{ij}}{k_{ij}} - u_{ij} \cos\theta_{ij} - v_{ij} \sin\theta_{ij}]$$

$$B_{ij} = \frac{\sin\theta_{ij}}{\Delta y} - \frac{\cos\theta_{ij}}{\Delta x} - \frac{1}{A_{ij}} (u_{ij} \sin\theta_{ij} - v_{ij} \cos\theta_{ij})(\frac{\cos\theta_{ij}}{\Delta y} + \frac{\sin\theta_{ij}}{\Delta x})$$

$$\overline{\frac{1}{k_{ij}} \frac{\partial k_{ij}}{\partial x}} =$$

$$\frac{-[\cos\theta_{ij} \frac{\partial u_{ij}}{\partial x} + \sin\theta_{ij} \frac{\partial v_{ij}}{\partial x}] - [\frac{\sigma_{ij} - u_{ij} k_{ij} \cos\theta_{ij} - v_{ij} k_{ij} \sin\theta_{ij}}{\sinh(2k_{ij} d_{ij})}] \frac{\partial d_{ij}}{\partial x}}{A_{ij}}$$

$$\frac{1}{k_{ij}} \frac{\partial k_{ij}}{\partial y} =$$

$$\frac{-[\cos\theta_{ij} \frac{\partial U_{ij}}{\partial y} + \sin\theta_{ij} \frac{\partial V_{ij}}{\partial y}] - [\frac{\sigma_{ij} - U_{ij} k_{ij} \cos\theta_{ij} - V_{ij} k_{ij} \sin\theta_{ij}}{\sinh(2 k_{ij} d_{ij})}] \frac{\partial d_{ij}}{\partial y}}{A_{ij}}$$

The computation is carried to the extent

$$|\theta_{new} - \theta_{old}| \leq 0.001 \, |\theta_{new}|$$

Since forward difference is used in the x-direction and backward difference is used in the y direction, θ needs to be specified at the offshore boundary and at the x-axis. The offshore boundary condition is the input. The condition of the x-axis could be specified in such a manner that $\theta_{i1} = \theta_{i2}$ without introducing significant error if the longshore bottom variation in the vicinity of the x-axis is slow.

The above numerical scheme becomes unstable when $B_{ij} \to 0$. The exact stability criterion cannot be easily determined. However, using the null-current condition as a guideline, one arrives at the following condition:

$$\frac{\Delta y}{\Delta x} > \text{Tan } \theta_m \tag{18}$$

where θ_m is the maximum expected wave angle. For example, if the maximum wave angle is expected to be less than 60°, the ratio of $\Delta y/\Delta x$ should be larger than 1.7. The velocity and depth gradients required in the computation are determined by central difference, i.e.,

$$G_{ij} = \frac{\Delta \xi}{\Delta x_i} = \frac{\xi_{i+1,j} - \xi_{i-1,j}}{2\Delta x_i}$$

where ξ represents u, v or d and x_k is either x or y.
The gradients at the boundary are taken as equal to zero at offshore and both sides and as constant at the shoreline, that is

$$G_{1j} = G_{2j}$$

These boundary conditions can, of course, be easily altered to fit individual cases.

(2) The wave energy equation in finite difference form is,

$$[dE(k)]_{ij} = \frac{[dE(k)]_{i,j-1}(v + C_g \sin\theta)\,\Delta x - [dE(k)]_{i+1,j}(u + C_g \cos\theta)\Delta y}{(v + C_g \sin\theta)\Delta x - (u + C_g \cos\theta)\,\Delta y + Q_{ij}\,\Delta x\Delta y} \qquad (19)$$

where $Q_{ij} = \frac{\partial}{\partial x}(u + C_g \cos\theta) + \frac{\partial}{\partial y}(v + C_g \sin\theta) + \tau$

$$\tau = \sigma_{xx}\frac{\partial u}{\partial x} + \sigma_{xy}\left(\frac{\partial v}{\partial x} + \frac{\partial u}{\partial y}\right) + \sigma_{yy}\frac{\partial v}{\partial y}$$

$\sigma_{\alpha\beta}$ are as defined in Eq. (16).

Here all the values of u, v and θ are evaluated at (i,j).

Eq. (19) is solved through a row by row relaxation until

$$|H_{new} - H_{old}| \leq 0.01\,|H_{new}| \qquad (20)$$

Like the wave angle solution, the finite difference scheme is forward in the x-direction and backward in the y-direction. The boundary values are also defined in a similar manner in that the shoreward boundary is specified as input and the values on the x-axis is taken the same as the next column ($E_{i1} = E_{i2}$).

On the shoreward direction, the wave will eventually break, the dissipation term ε in Eqs. (14) can no longer be neglected. If dissipation is not allowed for, the wave energy density will keep increasing and the numerical solution will eventually become unstable. Therefore, a constraint must be built in to restraint super saturation of energy flux. Since the real mechanism of energy dissipation is not well understood. An empirical criterion based upon total wave energy in terms of significant wave height is employed here, such that the height is restricted by the following condition (Divoky, et al., 1970)

$$\left(\frac{H_S}{L_S}\right)_b = 0.12 \tanh 2\pi \left(\frac{d}{L_S}\right)_b \qquad (21)$$

where the subscript b refers to breaking condition and H_S is related to the total wave energy in the conventional expression:

$$H_S = 2.828 \sqrt{E} \tag{22}$$

This criterion is to be further examined in later section when we have the field data in hand.

The input requirements includes a grid of water depth augmented by the tidal condition. The grid size should be selected in accordance with the criterion set in Eq. (18). Strictly speaking, directional spectra of the form $\phi_B(n,\theta)$ should be prescribed along the seaward boundary. Since our present knowledge on directional spectrum is quite inadequate, the program will also accept one-dimensional spectra as the input. The directional information should then be provided as predominant wave angles at each grid point along the outer boundary.

4. Field Program

The field experiments were conducted at the Island of Sylt, West Germany. The site location and area hydrograph are shown in Fig. 4. The site is exposed to the North Sea and is characterized by the existance of an underwater transverse ridge (a pronounced sand bar) running parallel to the shore approximately 500 m from the shoreline. This underwater sand bar is not stationary but frequently is shifting its location from season to season and sometimes after a major storm. Apparently influenced by this ridge, the nearshore flow-pattern and the resulting nearshore bottom topography become rather complicated. Shallow scouring pits, often appearing in eddy-like pairs, dotted the area at uneven spaces. Since the normal tidal range is 2 m in this area and the normal water depth over the ridge is only of the order of 3 m, waves often break over the ridge and reform afterwards.

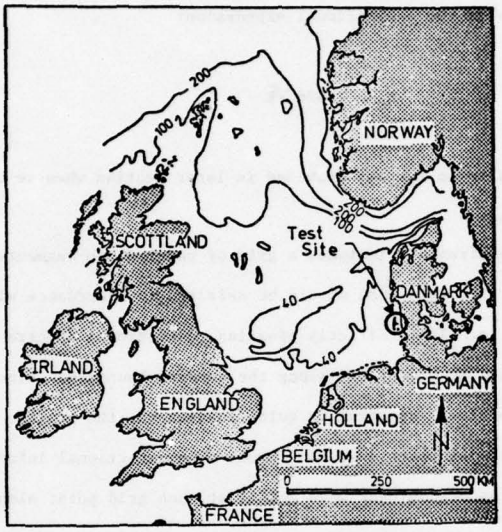

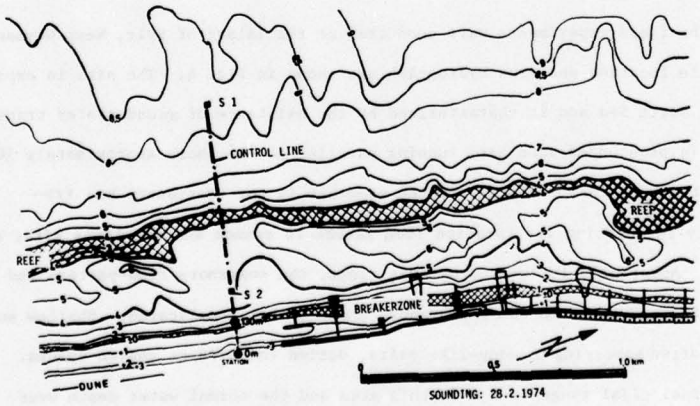

Fig. 4: Site location and area hydrograph

To measure the change of wave characteristics over this region, seven wave gages were installed at locations as shown in Fig. 5. Gages 1 and 2, which were bottom-mounted in relatively deep water, were echo-transceivers as developed by Fuhrentholz Laboratory (See Reference). These echo sounders were capable of measuring water surface variations to $\pm$ 0.5 cm for water depth up to 90 m. The shallow water gages (3 to 7) were staff-mount pressure transducers of Type MDS76 as manufactured by H. Maihak AG, Hamburg with a pressure range of 0-1 kg/cm^2. Gages 1 to 5 were installed perpendicular to the shoreline to measure the wave spectra transformation over the ridge and in shoaling water. Gages 5 to 7 were mounted parallel to the shoreline to measure mainly the wave approaching angle.

Wave data were collected from May 1 to May 15, 1976 at selected times to cover various combinations of tidal stages, waves approaching angles and wind conditions. Data were transmitted to shore station by underwater cable and were recorded simultaneously on FM analog magnetic tape and strip charts. During the course of wave measurement, currents were also measured with two-component electromagnetic current meters mounted at Gage stations 2 and 5. Variable-depth drogues were also deployed at times to determine the current condition. Description of instrumentation and recording devices was presented by Führböter and Büsching (1974).

5. Data Analysis

Wave energy spectra--Spectral analysis was performed using FFT (Fast Fourier Transform) technique developed by Cooley and Tukey (1965) with a Hanning Window (Black and Tukey, 1958) for data smoothing. All the data sets were sampled uniformly at a time interval Δt = 0.25 seconds to a total data points N = 2048 (or 512 seconds data period). These values were chosen to cover adequately waves with

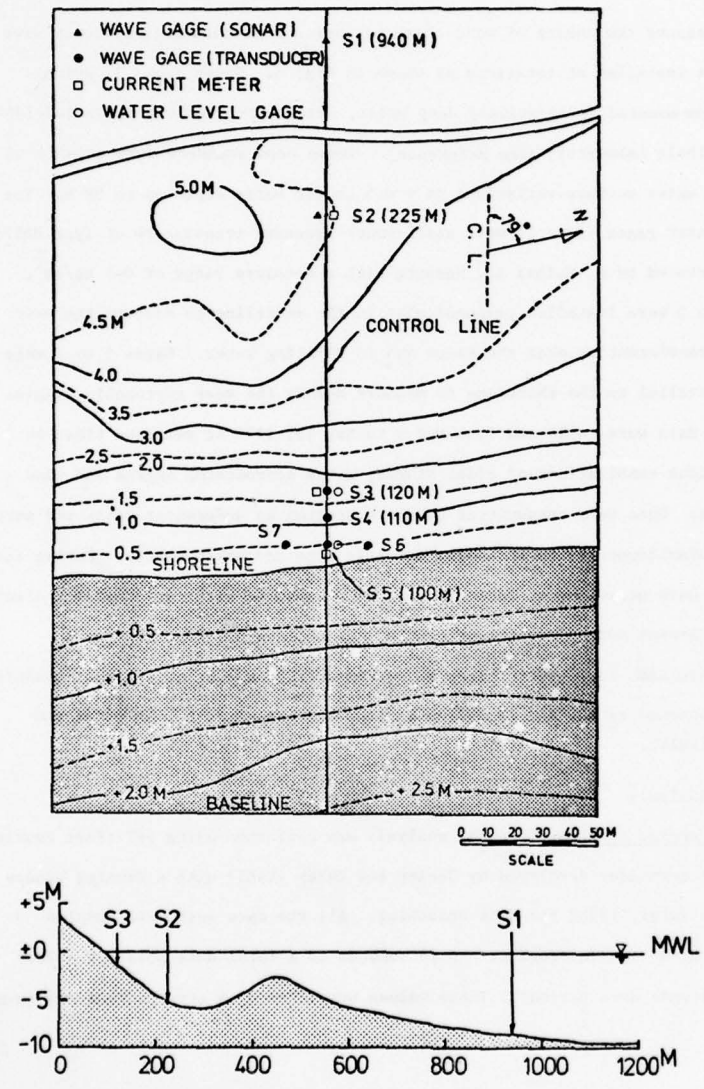

Fig. 5: Gage locations and nearshore hydrograph

periods ranging from two to nine seconds which were determined (as the range of energy containing waves) through visual examination of the data record and the wind condition during measurements. A section of data sample is shown in Fig. 6.

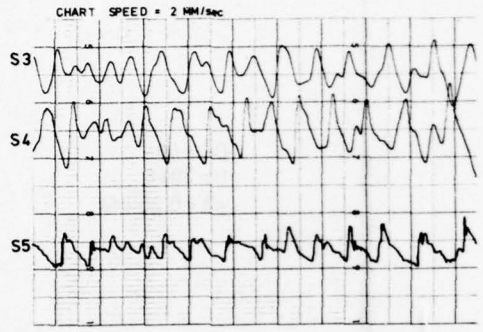

Fig. 6: Sample of wave data

After several trial runs, a degree of freedom DF = 40 was selected as the optimum to yield sufficiently smooth spectral curves to facilitate comparisons with theoretical prediction, yet, at the same time to preserve sufficient detail to truthfully portray the actual conditions. Figure 7 shows a comparison between the periodogram and the smoothed spectrum.

Data collected in shallow water by gages 3 to 7 were actually wave pressure instead of the true water surface fluctuations. To derive the energy spectra from the measured pressure signals, the depth attenuation effect needs to be compensated according to the relation:

$$S(f) = \left[\frac{\cosh kd}{\cosh k(d-\ell)}\right]^2 S_p(f) \qquad (23)$$

where $S_p(f)$ is the pressure spectral density as obtained; ℓ is the depth of the transducer measured from mean water level.

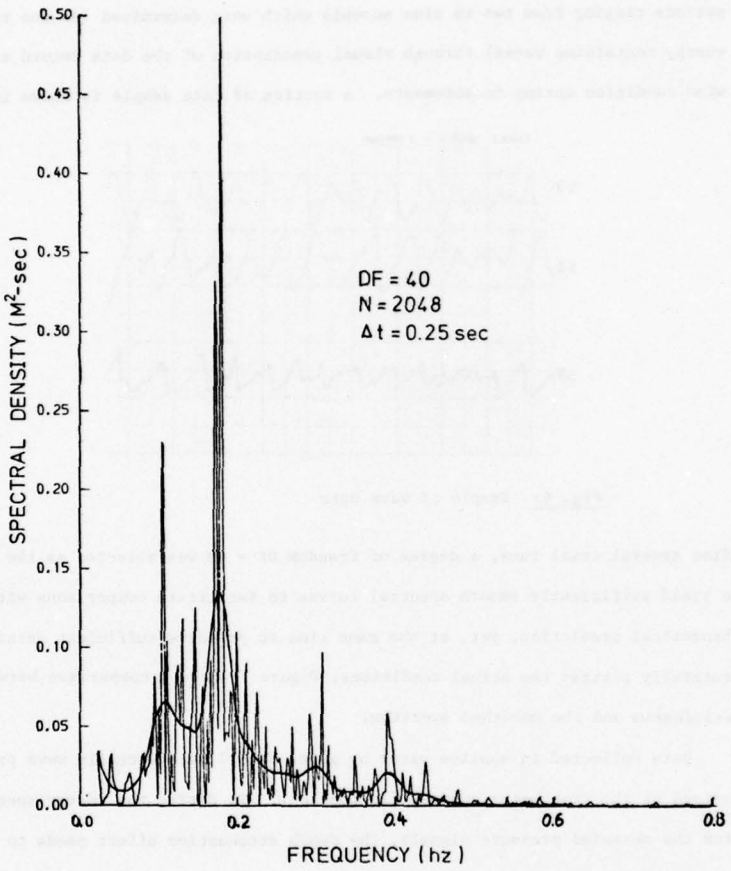

Fig. 7: Comparison between periodogram and smoothed spectrum

This correction factor is based upon linear wave theory and it tends to over compensate high frequency components which were more or less contaminated by

noise. An attempt was made to apply this correction factor to data analysis and was later abandoned because such corrections did little to wave components in the energy containing range but grossly over amplifying the high frequency components.

Wave approaching angle--To calculate the transformation of wave spectra, one requires to prescribe the one-dimensional wave spectra in frequency or period domain as well as the directional characteristics at the outer boundary. Based upon the computational method suggested here, the directional information should be expressed in terms of dominant angle of approach and if desirable a predesignated spreading function. Since the present field set-up yielded no directional information at the deep water sites, an alternative method was used which utilizes the information obtained from the shallow water gage arrays. As illustrated in Fig. 8 when a wave front passing by a cluster of three wave gages set

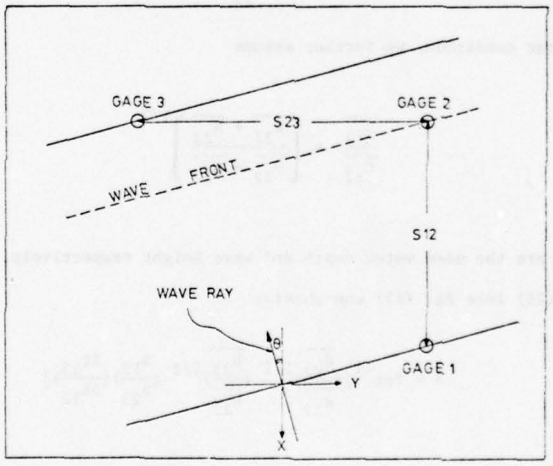

Fig. 8: Shallow water gage arrays for directional information

apart with known, but small distances, the following relations are approximately valid:

$$\overline{C}_{12}\,\Delta t_{12} = S_{12}\cos\theta$$
$$\overline{C}_{23}\,\Delta t_{23} = S_{23}\sin\theta \qquad (24)$$

where $\overline{C}$ is the mean wave celerity; S is the horizontal distance; Δt is the time span for wave front travelling from one wave staff to the other and θ is the wave approaching angle. The indices 1, 2 and 3 indicate the gage numbers. The above equation when solved for angle θ, yields

$$\theta = \mathrm{Tan}^{-1}\left[\left(\frac{S_{12}}{S_{23}}\right)\left(\frac{\overline{C}_{23}}{\overline{C}_{12}}\right)\left(\frac{t_{13}}{t_{12}}\right)\right] \qquad (25)$$

For shallow water condition, we further assume

$$\frac{\overline{C_{23}}}{\overline{C_{12}}} = \left[\frac{\overline{d_{23}} + \overline{H_{23}}}{\overline{d_{12}} + \overline{H_{12}}}\right]^{1/2} \qquad (26)$$

where d and H are the mean water depth and wave height respectively. Substituting Eq. (26) into Eq. (25) one obtains

$$\theta = \mathrm{Tan}^{-1}\left[\left(\frac{\overline{d_{23}}}{d_{12}}\right)^{1/2}\left(\frac{\overline{H_{23}}}{H_{12}}\right)^{1/2}\left(\frac{S_{12}}{S_{23}}\right)\left(\frac{\Delta t_{13}}{\Delta t_{12}}\right)\right] \qquad (27)$$

Since d and S are known, H and t can be measured off directly from the wave

records as illustrated, the angle of approach θ can be computed. The deepwater wave angle θ_o was then determined by conventional wave refraction computation for the dominant wave component or components.

6. Field Results

A selected set of data were presented here to demonstrate the spectral transformation under various combinations of wave incident angle, wind condition and tidal stage. Table 1 summarizes the cases reported. The wind record during the measuring period is displayed in Table 2. Figures 9 to 15 plot the wave spectra as measured at various gage stations along the control line for each case reported herein. The estimated wave and swell approaching angles and the wind directions are shown in Fig. 16. The wind direction is defined in terms of the dominant direction over an 8-hour period prior and up to the measuring time. The directional variations over this period are also included in Fig. 16. Of the seven cases, 1,6 and 7 are mainly wind waves as clearly revealed by the shape of the spectra; the wave approaching angles all coincide with the wind direction. Cases 3 and 5 are dominated by swell; the wind direction and wave angle bears no relation. Finally, cases 2 and 4 represent mixed swell and sea condition such that the wave angles are also mixed. In Case 2, for instance, the directions of swell and sea are almost perpendicular to each other.

The offshore shoal apparently plays an important role in the wave energy transformation mainly because the water depth is only 2.5 m at the crest of the shoal (see Fig. 5) but the tidal range is of the order of $\pm$ 1 m. Thus,

Table 1: Summary of field conditions

No.	Date	Wind U(m/s)	Wind α	Tide (m)	Wave Angle*		$H_{1/3}$** (m)		$E(10^{-2}F^2s)$**	
1	May 3 15 : 45	4-6	SSW	+0.82	θ_1	-12°	H_1	0.67	E_1	5.58
					θ_2	-15°	H_2	0.69	E_2	5.90
					θ_3	-18°	H_3	0.37	E_3	1.70
2	May 5 11 : 00	5-7	WSW	-1.30	θ_1	$+7^\circ$	H_1	0.99	E_1	12.30
					θ_2	$+12^\circ$	H_2	0.61	E_2	4.67
					θ_3	-10°	H_3	-	E_3	-
3	May 5 16 : 15	3-5	WSW	+0.53	θ_1	$+12^\circ$	H_1	1.04	E_1	13.52
					θ_2	$+10^\circ$	H_2	1.08	E_2	14.47
					θ_3	$+13^\circ$	H_3	0.85	E_3	8.95
4	May 6 14 : 50	3	W	-0.25	θ_1	$+12^\circ$	H_1	0.67	E_1	5.63
					θ_2	$+10^\circ$	H_2	0.59	E_2	4.35
					θ_3	$+13^\circ$	H_3	0.46	E_3	2.68
5	May 7 18 : 00	6	E	+0.33	θ_1	$+9^\circ$	H_1	0.54	E_1	1.43
					θ_2	$+11^\circ$	H_2	0.32	E_2	1.27
					θ_3	$+9^\circ$	H_3	0.20	E_3	0.49
6	May 11 10 : 15	8-9	W	+1.00	θ_1	-17°	H_1	1.39	E_1	24.30
					θ_2	-11°	H_2	1.16	E_2	17.10
					θ_4	-9°	H_4	1.34	E_4	22.70
7	May 11 16 : 20	6-7	WSW	-1.10	θ_1	-17°	H_1	0.63	E_1	8.60
					θ_2	-11°	H_2	0.62	E_2	4.87
					θ_4	-9°	H_4	-	E_4	-

*Wave Orthogonal with respect to Control Line, + clockwise, - counterclockwise

**The number indicates station as shown in Fig. 5

$$E = \frac{1}{2} \sum_{n=1}^{N/2} a_n^2 + b_n^2 \quad ; \quad H_{1/3} = 2.828 \sqrt{E}$$

DATE / WIND TIME	MAY 1, 76		MAY 2, 76		MAY 3, 76		MAY 4, 76		MAY 5, 76		MAY 6, 76		MAY 7, 76		MAY 8, 76		MAY 9, 76		MAY 10, 76		MAY 11, 76		MAY 12, 76		MAY 13, 76		MAY 14, 76		MAY 15, 76	
	Speed (m/s)	Direc-tion	Speed (m/s)	Direc-tion	Speed (m/s)	Direc-tion	Speed (m/s)	Direc-tion	Speed (m/s)	Direc-tion	Speed (m/s)	Direc-tion	Speed (m/s)	Direc-tion	Speed (m/s)	Direc-tion	Speed (m/s)	Direc-tion	Speed (m/s)	Direc-tion	Speed (m/s)	Direc-tion	Speed (m/s)	Direc-tion	Speed (m/s)	Direc-tion	Speed (m/s)	Direc-tion	Speed (m/s)	Direc-tion
01	7.06	WSW	4.53	SSE	3.14	SSW	10.78	-	10.58	WSW	3.69	ENE	3.72	NE	5.83	E	2.25	WNW	5.11	ENE	4.83	*	3.69	SW	11.28	WSW	15.81	WSW	2.19	SW
02	6.83	"	4.69	SE	3.81	"	10.17	-	10.89	"	3.58	"	4.19	ENE	7.53	ESE	3.19	N	5.14	"	8.89	WNW	3.47	SSW	10.56	"	14.94	"	1.36	"
03	6.06	"	4.94	S	5.56	"	11.83	-	10.33	"	4.58	"	4.03	"	8.11	"	3.14	NNE	5.28	"	8.75	W	3.50	S	9.33	SW	14.81	"	.86	ENE
04	5.81	"	6.86	SSW	6.94	SW	13.56	-	9.17	"	4.61	"	3.28	"	7.86	"	3.19	NE	5.25	"	9.28	WNW	4.92	"	8.56	"	13.64	"	1.53	"
05	6.17	"	6.00	SW	7.94	"	12.56	-	8.50	"	3.97	"	3.89	"	7.22	"	2.94	"	5.03	"	8.89	"	4.89	"	9.08	"	12.89	"	2.06	"
06	6.06	"	4.11	"	5.25	"	10.86	-	7.50	W	3.06	"	3.47	"	7.14	"	3.50	ENE	4.69	"	9.42	"	5.97	"	10.22	"	13.14	"	2.50	"
07	6.56	"	5.33	"	5.64	"	11.72	-	7.00	WNW	3.14	"	2.58	"	6.67	SE	3.22	NE	5.11	"	8.44	"	6.56	"	10.50	"	13.14	"	2.97	"
08	6.81	"	6.36	"	6.44	"	15.00	-	6.08	WSW	2.89	"	3.50	"	5.81	"	2.25	NNE	5.78	"	8.67	W	6.97	SSW	11.17	"	12.11	"	3.33	"
09	7.39	"	6.72	"	5.97	SSW	14.75	-	6.36	"	1.89	"	4.28	E	3.97	SSE	3.22	NE	6.03	"	7.56	"	8.00	"	11.81	"	12.92	"	3.03	E
10	7.33	"	6.69	SSW	6.97	"	14.44	WSW	5.42	"	1.50	*	5.06	ESE	4.94	SSW	2.81	ENE	6.56	"	8.00	"	8.42	"	11.47	WSW	11.47	"	2.78	SE
11	5.86	"	8.58	"	6.03	SW	14.61	"	4.56	"	2.42	N	5.31	ENE	4.42	SSE	3.33	"	6.75	E	7.86	WSW	9.00	"	12.36	"	9.97	"	3.14	"
12	4.58	"	9.19	"	5.83	SSW	14.31	"	3.83	"	3.89	NNW	5.47	ESE	4.92	"	4.36	"	7.56	ESE	7.03	"	8.33	"	13.97	"	7.75	"	3.69	"
13	4.31	"	8.58	"	6.33	"	11.69	"	3.86	"	4.39	"	5.92	E	4.81	"	4.72	"	8.39	"	6.83	"	8.75	"	14.78	"	7.44	"	3.61	"
14	4.72	"	8.75	"	5.58	SW	11.64	"	4.17	"	6.22	N	5.64	"	5.00	SSW	3.86	"	8.14	"	6.44	"	8.22	"	14.83	"	7.06	"	3.69	"
15	3.67	SW	8.03	"	4.31	"	11.25	"	3.64	"	6.50	NNE	5.72	"	7.36	"	3.86	"	8.31	"	6.33	"	8.22	SW	15.03	"	5.39	"	3.97	"
16	3.42	"	8.64	SW	4.97	"	11.19	"	3.42	"	6.36	"	6.28	"	5.97	SW	3.67	"	7.67	"	6.00	"	6.47	"	15.17	"	5.92	"	3.81	SSE
17	3.00	"	7.61	"	3.44	"	11.00	"	1.67	"	5.89	"	7.11	"	2.92	WSW	3.78	ESE	6.72	E	4.67	"	5.67	SSW	16.06	"	5.69	"	3.83	"
18	3.14	"	7.19	"	2.56	SSE	11.11	"	1.22	"	5.81	"	6.58	ENE	1.58	"	3.31	*	7.28	ENE	4.08	"	7.00	SW	16.19	"	5.11	"	3.81	"
19	2.78	"	6.33	"	2.92	-	10.03	"	.89	*	6.14	"	6.06	"	1.36	W	4.67	ENE	6.81	"	3.81	"	6.83	"	14.08	"	5.19	"	3.81	SE
20	2.03	SSE	5.89	"	3.14	-	9.22	"	1.86	ENE	5.78	"	5.86	"	1.28	*	4.50	"	5.86	"	4.11	SW	5.64	"	13.53	"	4.94	"	2.61	E
21	2.67	"	5.06	"	3.19	-	8.08	"	2.56	"	5.47	"	6.44	"	1.33	*	5.25	"	5.69	"	3.81	"	3.92	S	13.75	"	3.72	"	2.86	ENE
22	3.69	"	4.22	"	3.42	-	8.06	"	2.97	"	5.50	"	6.44	"	1.19	*	5.58	"	5.56	"	4.22	"	4.67	SSE	14.53	"	2.47	"	4.17	"
23	4.03	"	4.08	"	4.06	-	9.58	"	3.06	"	4.00	NE	6.42	"	.67	*	5.67	"	5.58	E	4.42	"	5.86	"	13.86	"	2.61	"	5.03	E
24	3.94	"	4.08	"	8.53	-	10.92	"	3.61	"	3.67	"	5.92	"	2.06	*	5.25	"	3.92	*	3.97	"	9.44	SSW	15.28	"	2.25	"	5.53	"

*Gage unstable (no exact direction) - Gage break down

Table 2: Wind Data of Westerland Sylt, Germany

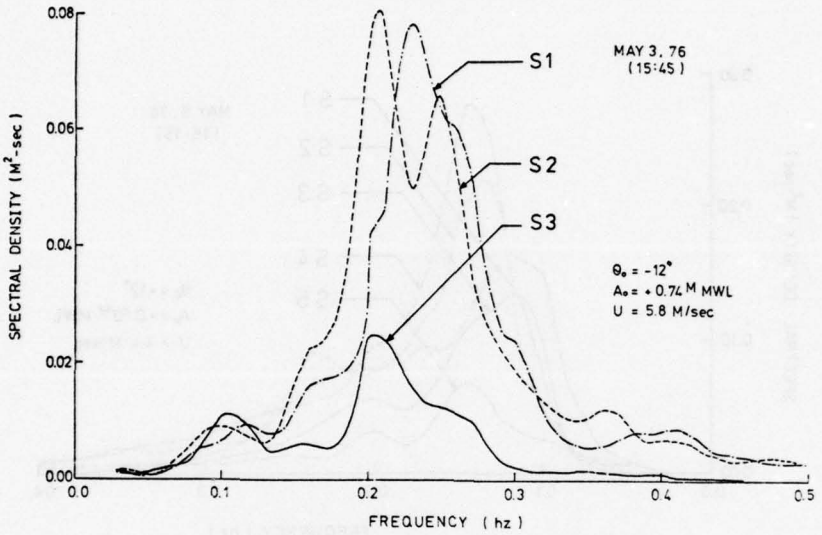

Fig. 9: Wave spectra measured on May 3, 1976 at 15:45

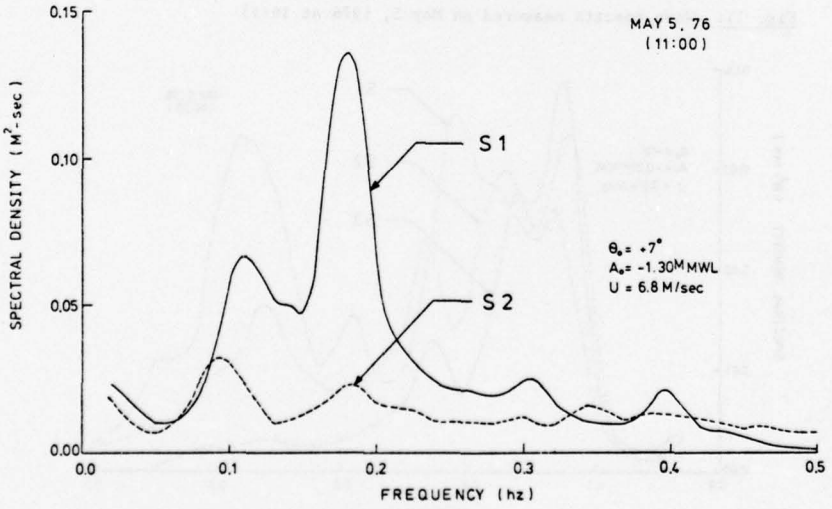

Fig. 10: Wave spectra measured on May 5, 1976 at 11:00

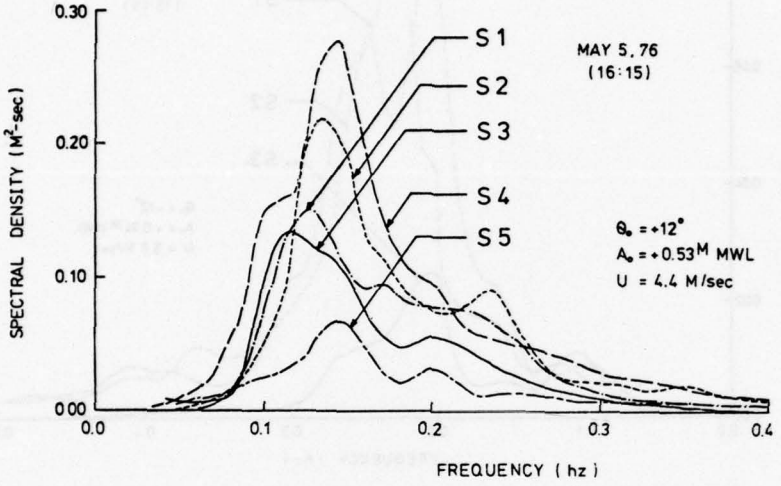

Fig. 11: Wave spectra measured on May 5, 1976 at 16:15

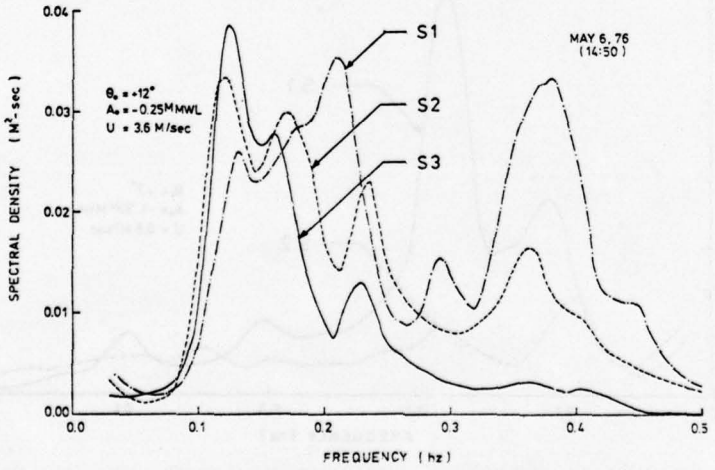

Fig. 12: Wave spectra measured on May 6, 1976 at 14:50

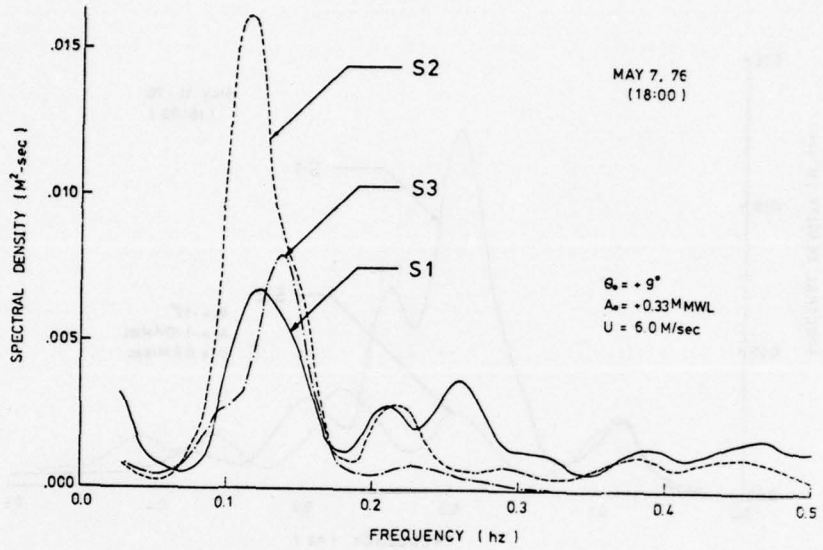

Fig. 13: Wave spectra measured on May 7, 1976 at 18:00

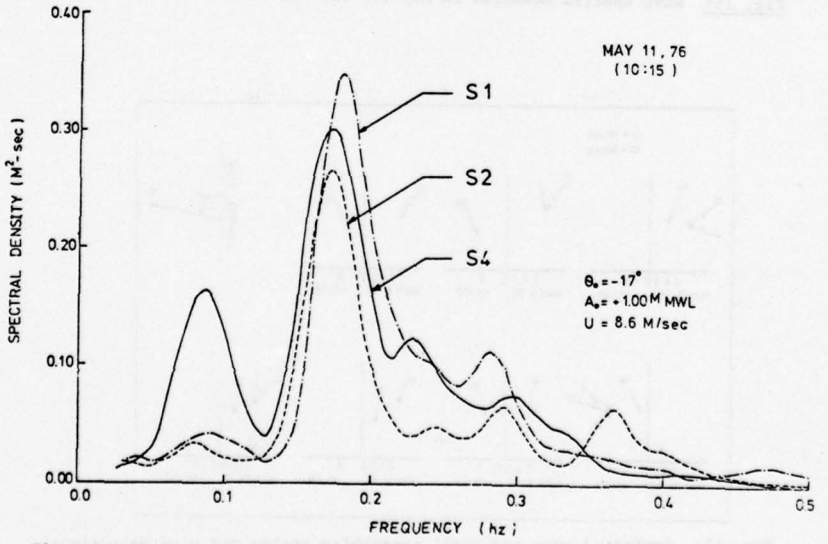

Fig. 14: Wave spectra measured on May 11, 1976 at 10:15

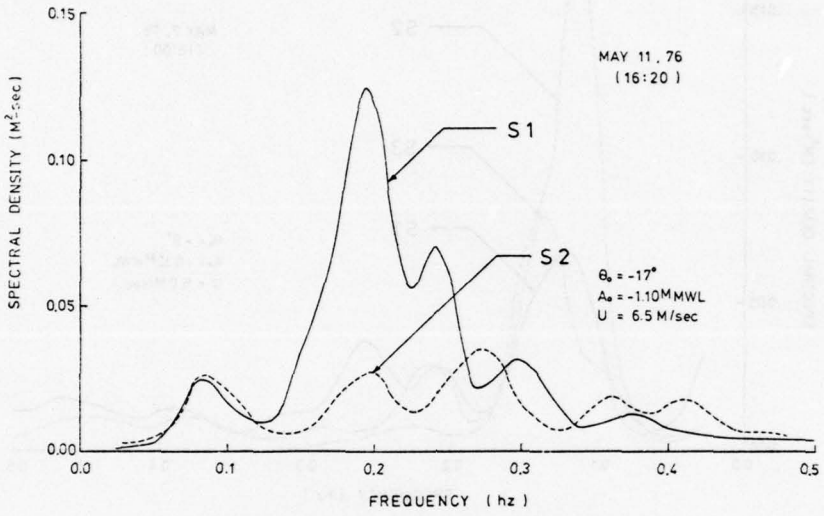

Fig. 15: Wave spectra measured on May 11, 1976 at 16:20

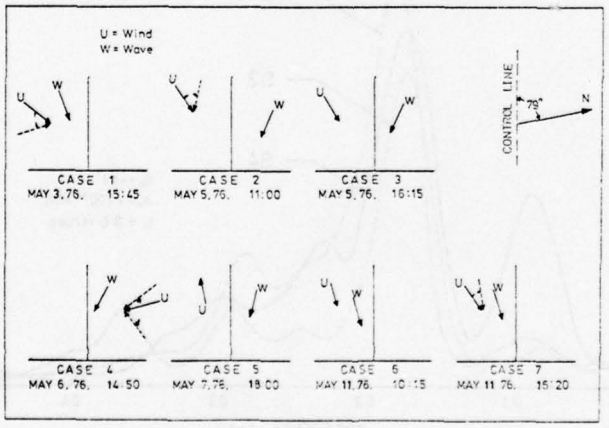

Fig. 16: Estimated wave and swell approching angles and wind directions

during low tide, it acts like a submerged breakwater. As the waves break over the shoal, a significant portion of wave energy is being dissipated. Wave components in the energy-containing range take the heaviest toll while the long wave components are less affected. The high frequency components remain largely intact and may actually show some gain, probably through reclaiming partially the energy lost by the main wave components. There is no indication that waves will reform after breaking. The dominant wave components will not recover their energy and their form. The appearance of the waves as well as the energy distribution among various frequencies are quite dissimilar on the two sides of the shoal. For nonbreaking situations, the shoal tends to attenuate the peaks of the spectra for onshore wind conditions. When the wind is offshore, on the other hand, the peak is significantly amplified (Case 5) due to the existance of the shoal. This is probably due to the combined effects of opposing current and the fact that energy generated by winds inshore of the shoal is being entrapped. This case will be further analyzed later.

In general, the energy spectra will peak further when approaching the shore before finally breaking. The total energy, however, tends to diminish somewhat in comparison with the offshore waves. Other measurements under storm conditions (Büsching, 1975) in the same area revealed similar results.

For the wind wave conditions, the JONSWAP spectra (Hasselmann, et al., 1973) which assume the following form quite adequately describe the offshore wave conditions:

$$E(f) = \alpha g^2 (2\pi)^{-4} f^{-5} \exp\left(-\frac{5}{4}\left(\frac{f}{f_m}\right)^{-4}\right) \gamma^{\exp\frac{-(f - f_m)^2}{2\sigma^2 f_m^2}} \qquad (28)$$

$$\sigma = \begin{cases} \sigma_a = 0.007 \text{ for } f \leq f_m \\ \sigma_b = 0.009 \text{ for } f < f_m \end{cases}$$

Containing five free parameters f_m, α, γ, σ_a and σ_b.
Here f_m represents the frequency at the maximum of the spectrum and the parameter α corresponds to the usual Phillips constant. The remaining three parameters define the shape of the spectrum: γ is the ratio of the maximum spectral energy to the maximum of the corresponding Pierson-Moskowitz (1964) spectrum

$$E_m(f) = \alpha g^2 (2\pi)^{-4} f^{-5} \exp(-\frac{5}{4}(\frac{f}{f_m})^{-4}] \qquad (29)$$

with the same values of α and f_m; σ_a and σ_b define the left and right side widths, respectively, of the spectral peak.

Although the JONSWAP spectra has 5 free parameters, among them, the peak enhancement factor γ is the only critical one that makes it differ from the P-M spectrum. Figures 17 to 20 offer some comparison among the data, the JONSWAP spectra and the P-M spectra.

7. Numerical Results and Comparison

One of the main purposes of this study is to compare the field results with the predictions based on the numerical technique developed. Before the computer program is applied to the actual field condition, a number of simple cases were computed to illustrate the general influence of bottom topography on spectrum transformation. First of all, a case against rhythmic hydrograph and shoreline (Fig. 21) is illustrated in Fig. 22 . The results clearly indicate, as expected, that the energy converges to the convex section of the shoreline (Point A) and diverges from the concave section of the beach. A case is then shown with a two-dimensional hydrograph that consists of a section of negative slope, i.e., the equivalent to an offshore bar. The resulting spectrum transformation is shown in Fig. 23. For this case, the energy

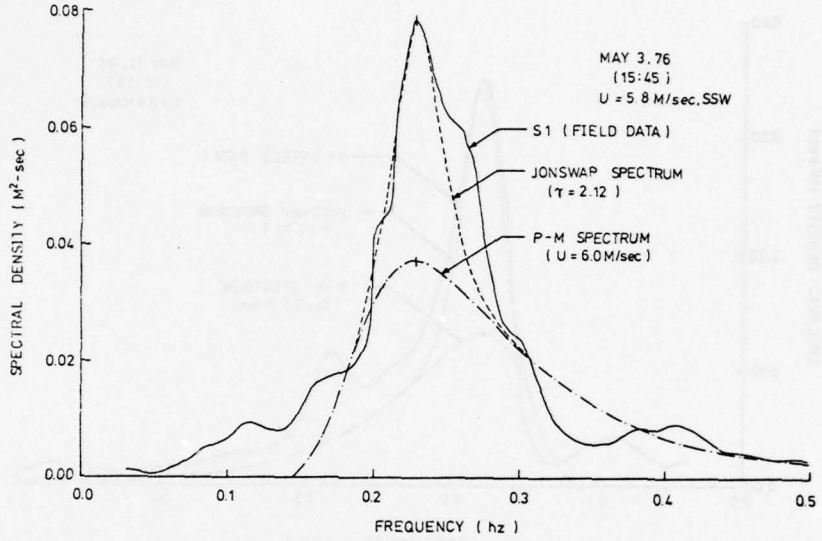

Fig. 17: Comparison among field data, JONSWAP and P-M spectra (Data from May 3, 1976 at 15:45)

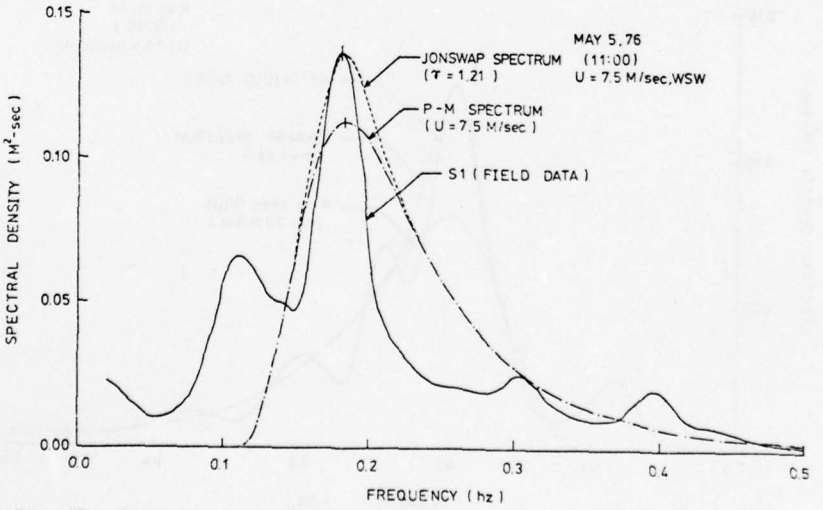

Fig. 18: Comparison among field data JONSWAP and P-M spectra (Data from May 5, 1976 at 11:00)

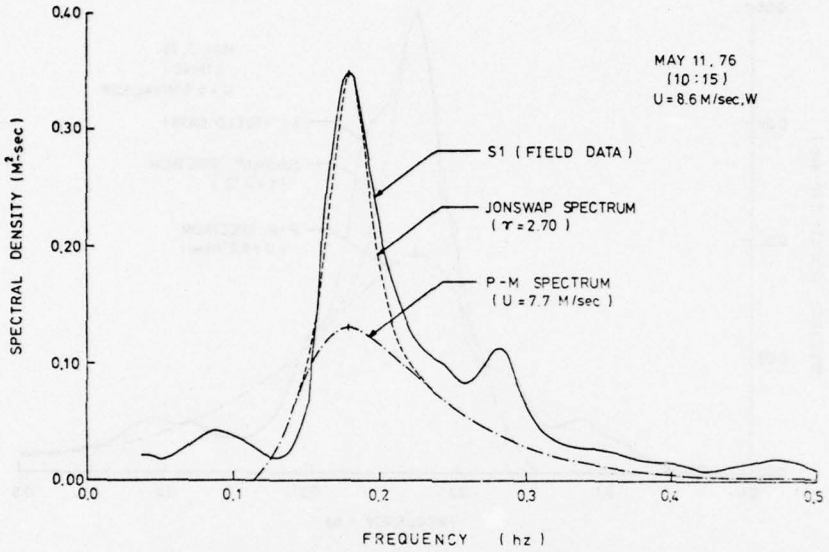

Fig. 19: Comparison among field data JONSWAP and P-M spectra (Data from May 11, 1976 at 10:15)

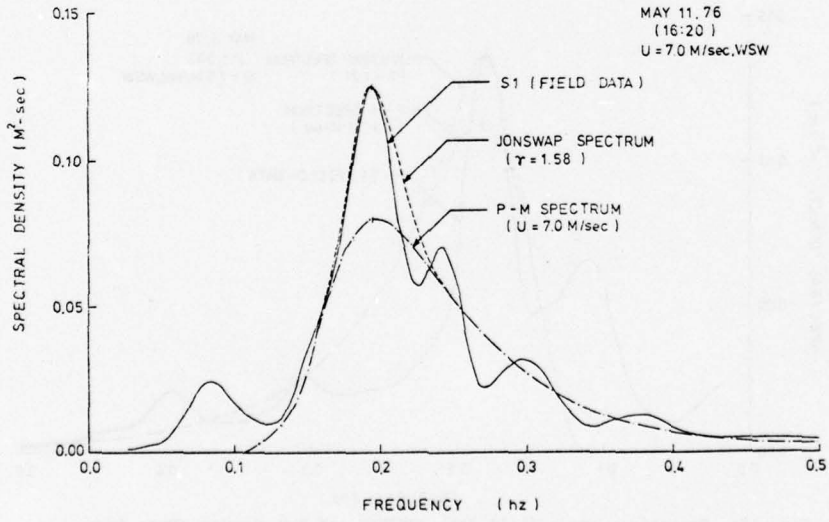

Fig. 20: Comparison among field data JONSWAP and P-M spectra (Data from May 11, 1976 at 16:20)

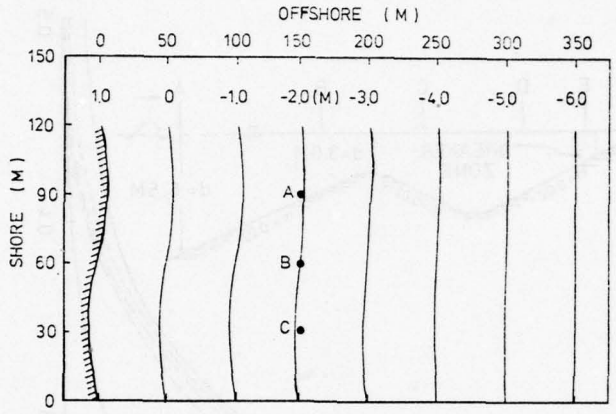

Fig. 21: Hypothetical rhythmic topography

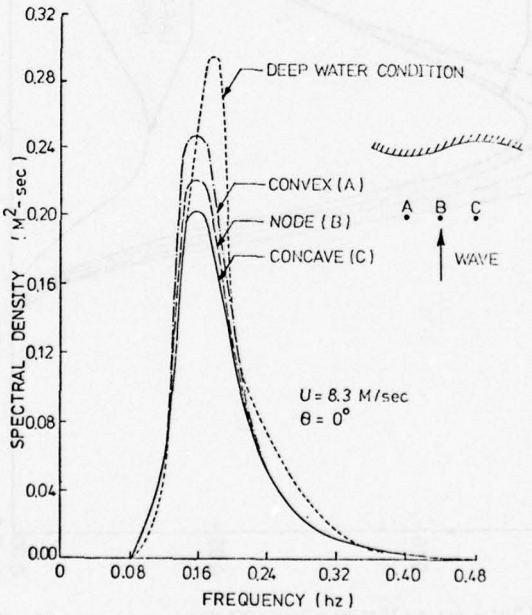

Fig. 22: Illustrations of spectral variations of wave spectrum over rhythmic topography

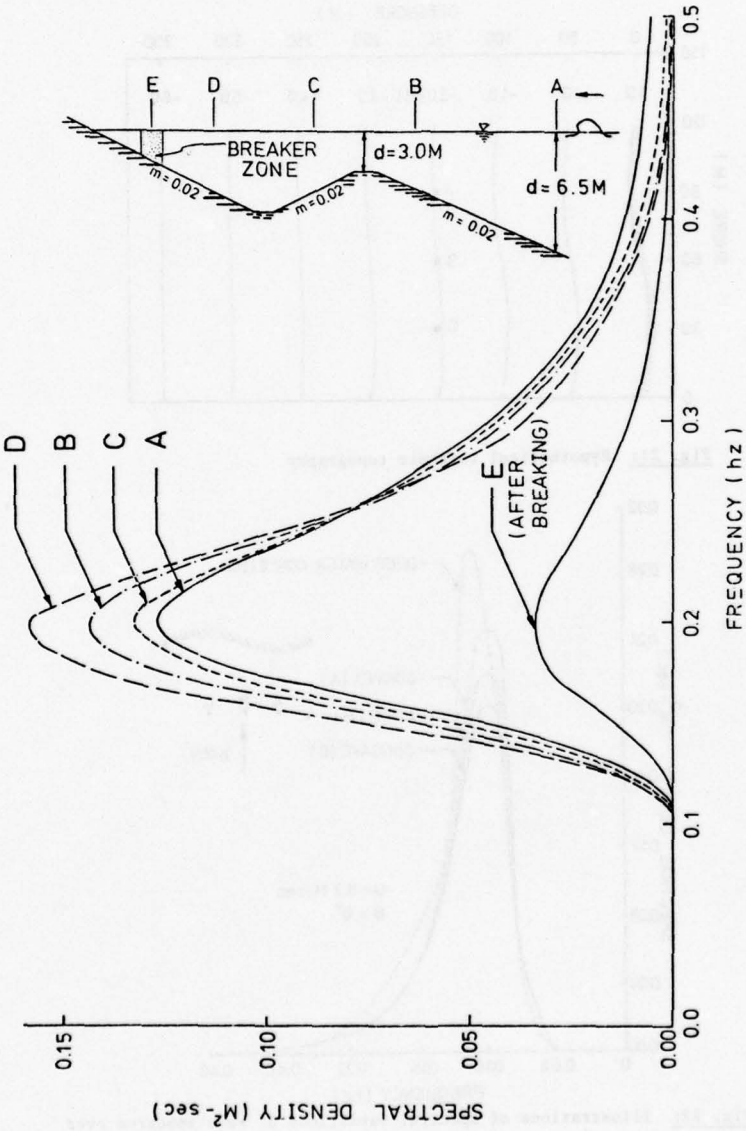

Fig. 23: Illustrations of spectral variations of wave spectrum over an offshore ridge

spectrum first peaks up on the positive slope before reaching the bar; the peak then diminishes in magnitude due to the effect of the negative slope before it increases again when the waves proceed towards the shore. Finally, (beyond the breaking point) the wave breaks and the spectrum diminishes both in intensity and in total energy.

Computations for the actual field condition were carried out for two different categories. In the first category, wave spectra as measured at S2 (225M from the baseline) were used as inputs to compute their transformations into nearshore zone close to the bench (S3 to S5). The bottom hydrograph used in this set of computations was based upon soundings taken during the period of field measurement. The input bottom-depth chart is shown in Fig. 24. Here the grid sizes are $\Delta x = 5m$ and $\Delta y = 20m$; the corresponding grid points are 36 and 11, respectively. Since the input wave spectrum was available at only one grid point where the spectrum was actually measured, the input along the rest of the offshore boundary need to be estimated. This was accomplished by first carrying the known spectrum as measured back to the deepwater condition. This deepwater condition is then assumed to be homogeneous over a horizontal dimension large enough to cover the width of the offshore boundary and thus allows to be used as the input to compute the boundary condition at the other grid points. This scheme, of course, allows only one exact match at the boundary point where the spectrum was actually measured.

Results of three representative wave-swell conditions are presented here; they are swell dominated condition (Case 3), swell-wave combined condition (Case 4), and wind-wave dominated condition (Case 6). Comparisons between the measured and computed spectra are summarized in Figs. 25 to 27, respectively, representing Cases 3, 4 and 6. In general, the prediction appears quite reasonable for wave components in the energy-containing range and low frequency range;

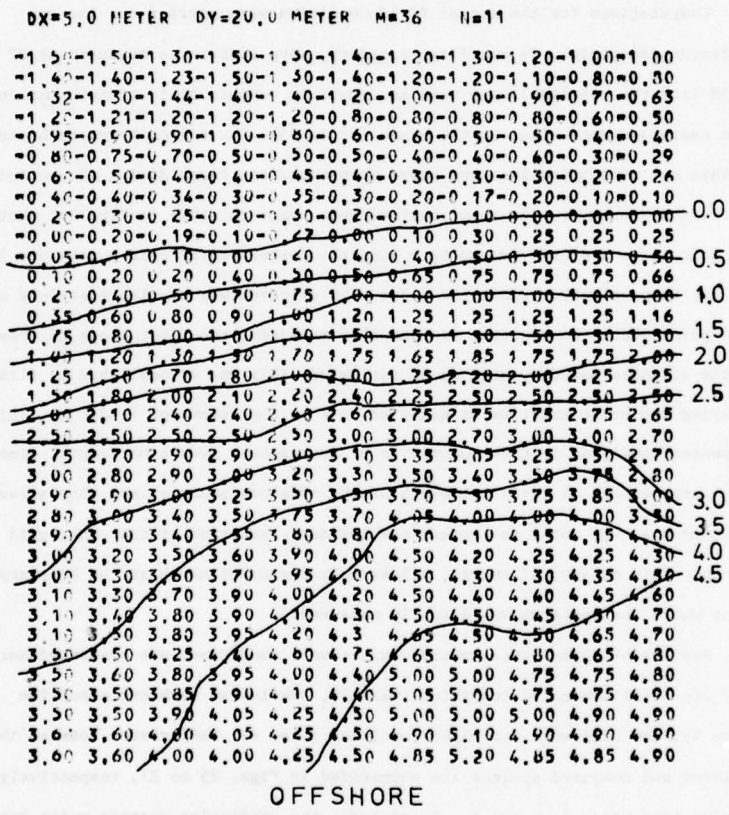

Fig. 24: The bottom-depth chart used as numerical input

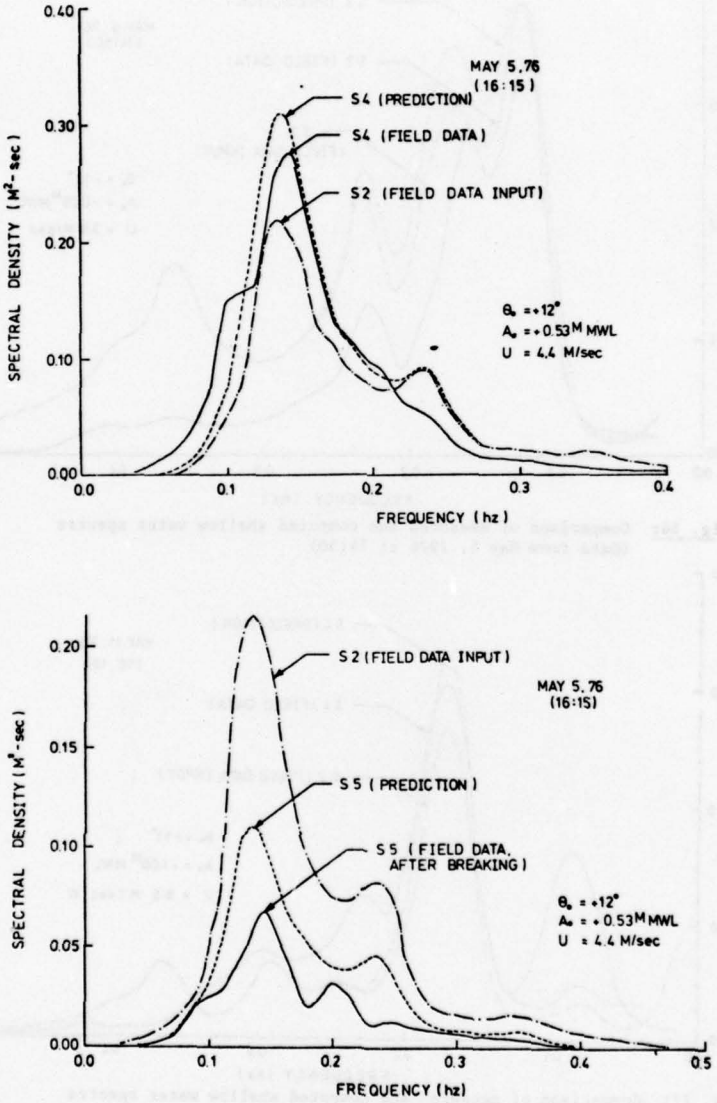

Fig. 25: Comparison of measured and computed shallow water spectra (Data from may 5, 1976)

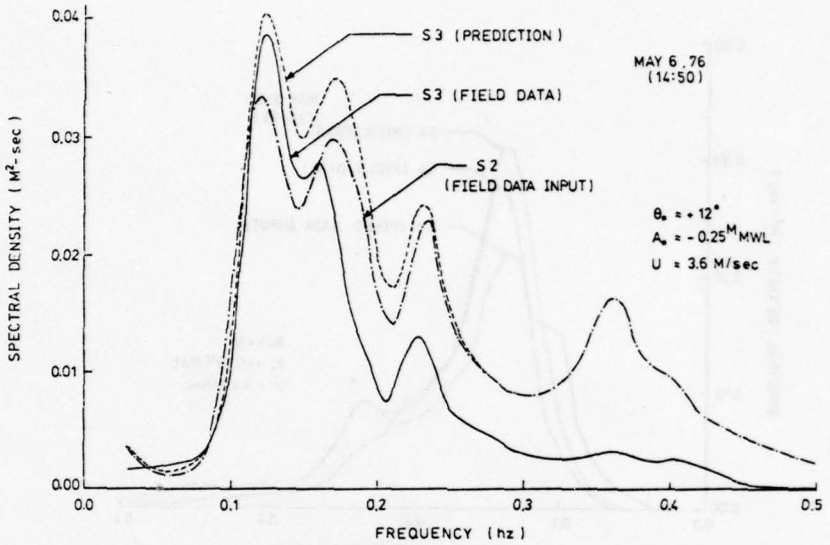

Fig. 26: Comparison of measured and computed shallow water spectra (Data from May 6, 1976 at 14:50)

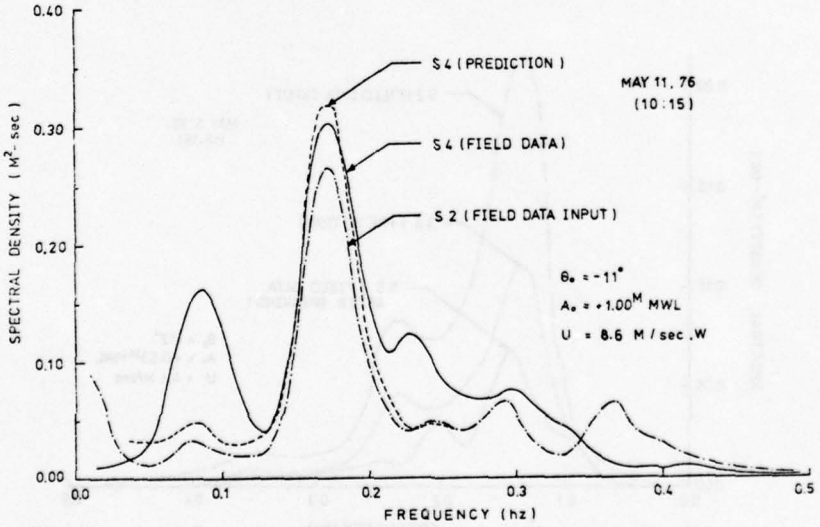

Fig. 27: Comparison of measured and computed shallow water spectra (Data from May 11, 1976 at 10:15)

in the high frequency range, the prediction becomes less desirable. Based on this observation, the wave components in the energy-containing range apparently are the most stable ones and are affected mainly by shoaling and refraction in their transformation prior to breaking. The slight over prediction at the spectral peak is most likely due to the fact that the nearshore wave data is actually pressure rather than surface variations and that no correction has been made to compensate this attenuation. For Case 3, the prediction was actually carried into the surf zone. The predicted spectrum after breaking appears quite reasonable (Fig. 25) both in order of magnitude and in shape. This limited result seems to support the breaking criterion expressed in Eq. (21).

A number of factors could contribute to the irregularity in the high frequency range. One possible source of error is that, in this range, the variations in spectral density as well as directions of propagation could be considerable and that results from one point measurement might be insufficient to provide a reasonable estimation of the input along the complete outer boundary. Also, the local generation and dissipation, which are most likely to affect wave components in this range, are not included in the model. There are at least some indications that such mechanisms might provide partial explanation on the discrepancy between measurement and prediction. In Case 6 (Fig. 27) wind is in the same direction as wave propagation, consequently, local generation tends to over-compensate dissipation, thus, resulting in a predicted value smaller than measured. On the other hand, in Case 4 (Fig. 26) when the wind direction was at a large angle with the wave direction, the prediction becomes larger than measured. It is possible that in this case, the locally generated wave was running against the predominant swell and thus resulted in considerable dissipation at high frequency range. A further examination on the energy dissipation criterion is presented in the subsequent section.

Numerical computations were also made for another category using measured data at S1 (940M from the baseline) as input to calculate the corresponding spectra at S2 to examine the wave transformation over the bar that lies between S1 and S2 as shown in Fig. 5. A much coarser grid system was used with x = 25 m and y = 75 m; the corresponding grid points are 19 and 11, respectively. Since no soundings were performed for such a large area (during the measuring period) the hydrograph is based upon the bottom depth chart of 1972, as supplied by the Leichtweiss-Institut fur Wasserbau, Braunschweig, Germany. Results are presented in Figs. 28 and 29. Figure 28 represents a case where waves approaching from N-W quadrant whereas the case shown in Fig. 29 is for waves coming from S-W direction. For these conditions, the prediction fares far better in the former case than the latter. A closer examination of the computer revealed that the spatial variations of wave spectrum are quite pronounced from grid to grid in both longshore and onshore-offshore directions for cases where waves come from the S-W whereas the contrary is true for waves from the N-W. This, at least partially explains why the prediction fares poorly for S-W waves. As a further illustration, the predicted spectral density function one grid distance from the actual location was also plotted in Fig. 29 for the S-W waves. The spatial sensitivity is apparent and is believed to be the main contributing factor to the poor correlation in this case. The fact that the predicted values are generally considerably higher than the measured for S-W waves seems to suggest that the offshore bar is a stronger wave reflector for waves approaching from this quadrant than that of the N-W quadrant.

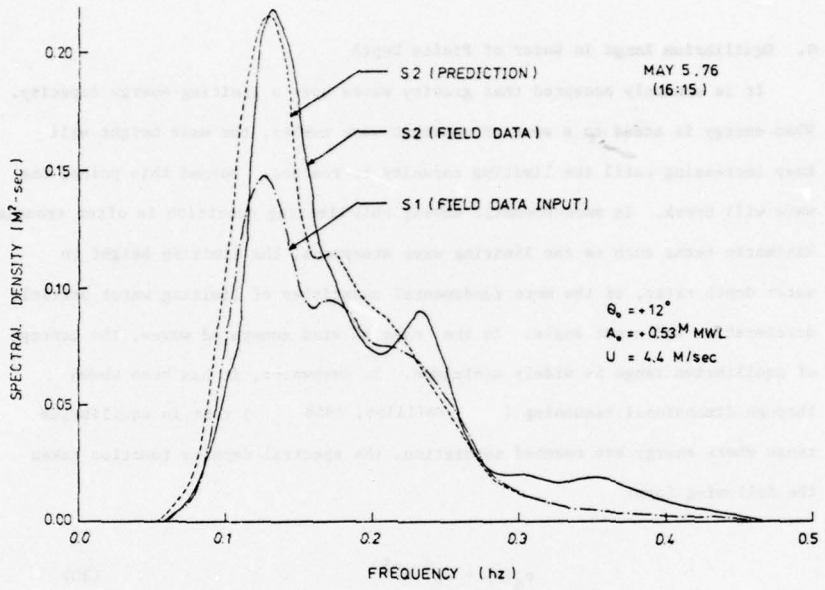

Fig. 28: Comparison of measured and computed deep water spectra (Data from may 5, 1976 at 16:15)

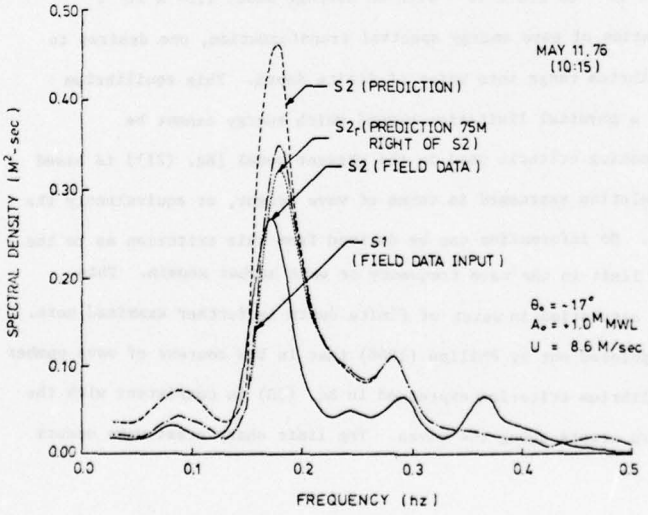

Fig. 29: Comparison of measured and computed deep water spectra (Data from May 11, 1976 at 10:15)

8. Equilibrium Range in Water of Finite Depth

It is commonly accepted that gravity waves have a limiting energy capacity. When energy is added to a wave of constant wave number, the wave height will keep increasing until the limiting capacity is reached. Beyond this point, the wave will break. In monochromatic waves, this limiting condition is often translakinematic terms such as the limiting wave steepness, the limiting height to water depth ratio, or the more fundamental quantities of limiting water particle acceleration and crest angle. In the case of wind generated waves, the concept of equilibrium range is widely acclaimed. In deepwater, it has been shown through dimensional reasoning (Phillips, 1958) that in equilibrium range where energy has reached saturation, the spectral density function takes the following form:

$$\phi_d(n) = \beta g^2 n^{-5} \tag{30}$$

where β, sometimes known as Philips constant, is determined from field data as ranging from 0.8×10^{-2} to 2.0×10^{-2} with an average about 1.17×10^{-2}.

In the computation of wave energy spectral transformation, one desires to extend this equilibrium range into water of finite depth. This equilibrium critiera provides a physical limitation beyond which energy cannot be retained. The breaking criteria used in the present model [Eq. (21)] is based on an empirical relation expressed in terms of wave height, or equivalently the total wave energy. No information can be derived from this criterion as to the energy saturation limit in the wave frequency or wave number domain. This problem of energy saturation in water of finite depth is further examined here.

It has been pointed out by Philips (1966) that in the context of wave number spectra, the equilibrium criterion expressed in Eq. (30) is consistant with the occurrence of sharp crests among the waves. The limit sharp crest wave occurs

when the local fluid acceleration at the surface exceeds a certain fraction of the gravitational acceleration, g. If we extend this physical reasoning to regions of shallow water by assuming that a certain wave component of wave number k_o will become saturated when the maximum vertical fluid acceleration at the surface reaches a critical value say, αg with α a constant of proportionality, the saturation criterion of this wave number component can then be expressed as

$$\frac{a_v}{g} = A_c(k_o)\, k_o \tanh k_o d = \alpha \tag{31}$$

based upon linear wave. Here a_v is the vertical particle acceleration and $A_c(k_o)$ is the limiting wave amplitude associated with the wave number, k_o. Since A is related to the wave energy, we further assume that

$$A_c^{\,2}(k_o) \propto \int_{k_o}^{\infty} g_a(k)\, dk = \gamma^2 \int_{k_o}^{\infty} g_a(k)\, dk \tag{32}$$

where $g_a(k)$ is the equilibrium one-dimensional wave spectrum integrated over the angle of spreading and γ is a constant of proportionality. The above assumption has the physical meaning that the contribution to wave steepness of a certain wave number component is mainly due to waves of higher wave numbers. The validity of this assumption may be illustrated in a much simplified situation with, say, two wave components of distinct wave numbers, k_1 and k_2, with, say, k_2 significantly larger than k_1, superimposing upon each other. One then expects that the effect of the longer wave on the shorter wave is mainly an apparent change of mean water level upon which the shorter wave rides. Neglecting the interaction between these two wave components, the steepness of the shorter wave can be considered to be unaffected by the longer one. The reverse, however, can not be true as any local irregularity as a result

of the superimposed shorter wave contributes to the change of wave steepness to the longer one. This argument when extended to irregular waves leads to the condition expressed in Eq. (32).

Now substituting Eq. (32) into Eq. (31), reveals that $g_a(k)$ should assume the following form

$$g_a(k) = 2\left(\frac{\alpha}{\gamma}\right)^2 \frac{kd\ \mathrm{sech}^2 kd + \tanh kd}{(k \tanh kd)^3} \tag{33}$$

This is the functional relationship of the spectral density in the equilibrium range $k_o > k$, in water of finite depth. Since $2\left(\frac{\alpha}{\gamma}\right)^2$ is a constant, a normalized function Ga(k) can be defined such that

$$G_a(k) = \frac{g_a(k)}{2\left(\frac{\alpha}{\gamma}\right)^2} = \frac{kd\ \mathrm{sech}^2 kd + \tanh kd}{k^3 \tanh^3 kd} \tag{34}$$

The function $g_a(k)$ or $G_a(k)$ is the counterpart of Eq. (30) for water of finite depth. The value of $k^3 g_a(k)$ approaches a constant when $d \to \infty$ as it should (see Phillips, 1966). For water of finite depth, however, $k^3 g_a(k)$ is a monotonically decreasing function of increasing kd. This relationship in terms of $k^3 G_a(k)$ vs. kd is shown in Fig. 30. The variation of $G_a(k)$ with kd is also computed and is shown in Fig. 31.

The constant in Eq. (33) can be estimated based upon the fact that when $d \to \infty$ the functional relationship expressed in Eq. (33) should approach Eq. (30), i.e.,

$$\lim_{d \to \infty} \int_{k_o}^{\infty} g_a(k)dk = \int_{n_o}^{\infty} \phi_d(n)dn \Big|_{n_o=\sqrt{gk_o}} \tag{35}$$

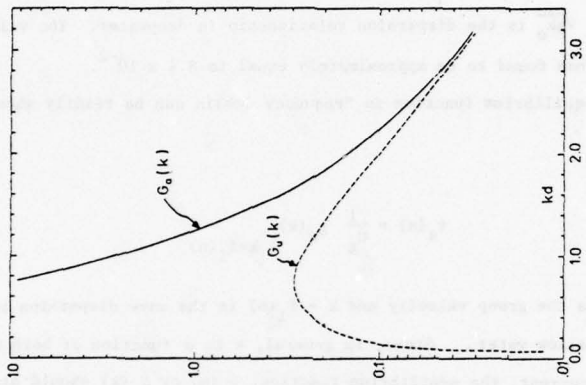

Fig. 31: Variation of Ga(k) and Gu(k) with kd

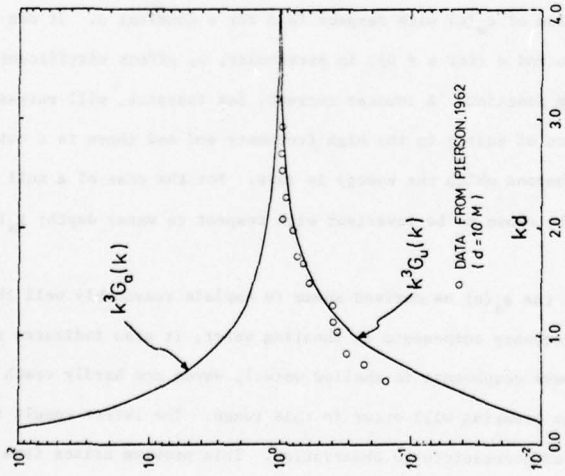

Fig. 30: Variation of k^3 Ga(k) and k^3Gu(k) with kd

where $n_o = \sqrt{gk_o}$ is the dispersion relationship in deepwater. The value of $2(\frac{\alpha}{\gamma})^2$ is thus found to be approximately equal to 8.4×10^{-2}.

The equilibrium function in frequency domain can be readily shown as

$$\phi_a(n) = \frac{1}{C_g} \left. g_a(k) \right|_{k=f_1(n)} \tag{36}$$

where C_g is the group velocity and $k = f_1(n)$ is the wave dispersion relationship in shallow water. Since, in general, k is a function of both water depth and current, the equilibrium function, $\phi_a(n)$ or $g_a(k)$ should also vary with these parameters. By virtue of Eq. (10) which is commonly accepted dispersion relationship, the variation of $\phi_a(n)$ or $g_a(k)$ with respect to both u and d can be easily established. Figures 32 and 33 plot the $\phi_a(n)$ as a function u keeping d constant. Figures 34 and 35, on the other hand, shows the variation of $\phi_a(n)$ with respect to d for a constant u. It can be seen that both u and d (for $u \neq 0$), in particular, u, affect significantly the equilibrium function. A counter current, for instance, will surpass a significant portion of energy in the high frequency end and there is a cut off frequency beyond which the energy is zero. For the case of a null current, $\phi_a(n)$ can be shown to be invariant with respect to water depth; $g_a(n)$, however, is not.

While the $\phi_a(n)$ as derived seems to explain reasonably well the behavior of high frequency components in shoaling water, it also indicates that for small kd (long wave components in shallow water), waves can hardly reach saturation and thus no breaking will occur in this range. The latter result indeed is puzzling and contradicts to observation. This problem arises from the basic

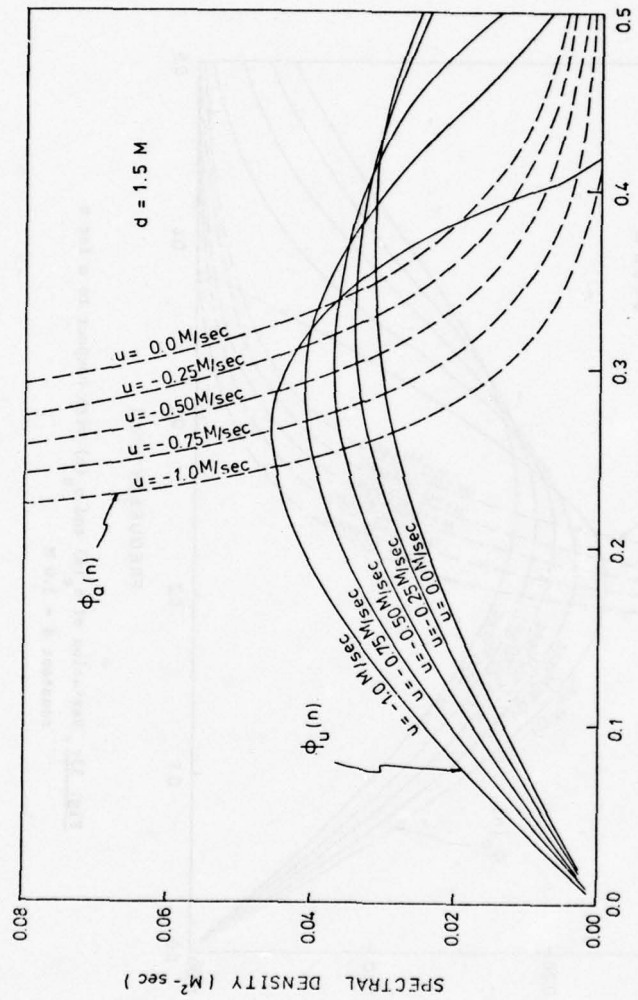

Fig. 32: Variation of $\phi_a(n)$ and $\phi_u(n)$ with respect to u for a constant d = 1.5 M

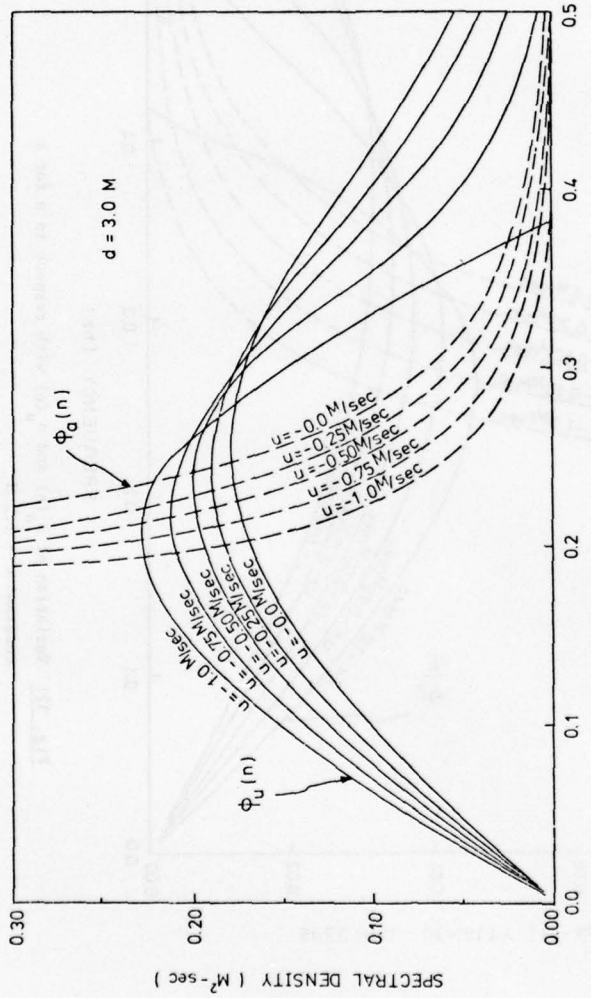

Fig. 33: Variation of $o_a(n)$ and $o_u(n)$ with respect to u for a constant d = 3.0 M

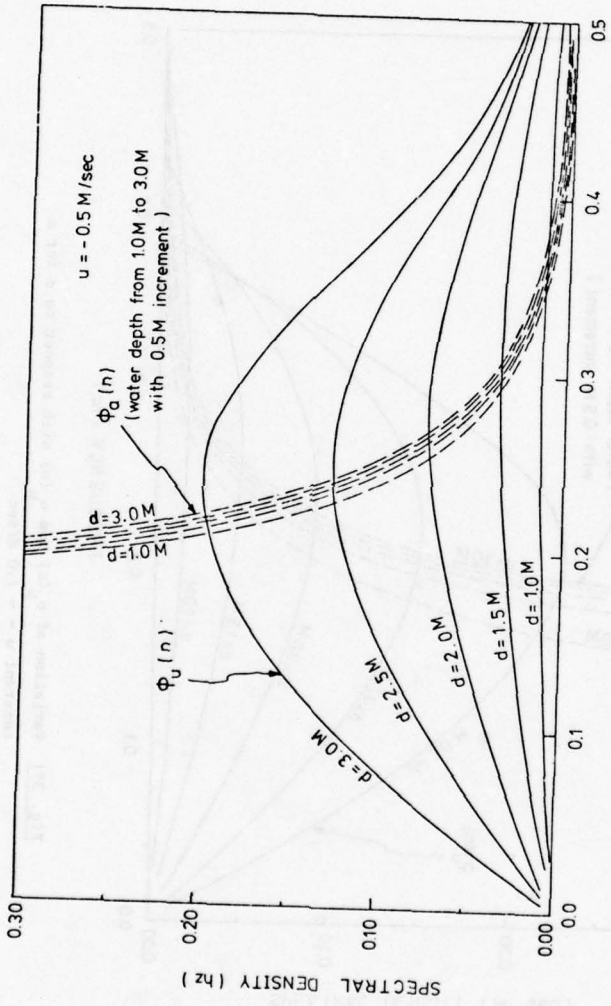

Fig. 34: Variation of $o_a(n)$ and $o_a(n)$ with respect to d for a constant u = - 0.5 M/sec

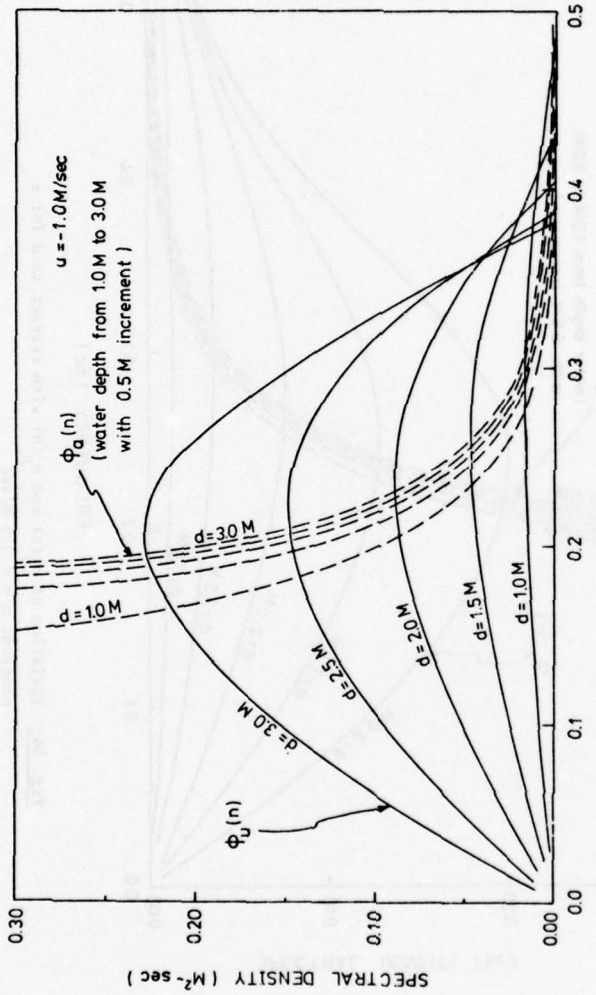

Fig. 35: Variation of $o_a(n)$ and $o_u(n)$ with respect to d for a constant u = - 1.0 M/sec

assumption in that the breaking criterion is based upon vertical acceleration. As waves enter into shallow region, the obitor water particle motion becomes elliptic. Thus, the fluid becomes more and more difficult to attain the critical vertical acceleration to reach incipient breaking. While the critical vertical acceleration might still remain as a sufficient condition, it no longer is necessary and the wave might break when other modes of motion exceed certain critical value. For wave components of small wave numbers in shallow water the fluid motion in the horizontal direction, both velocity and acceleration, becomes significantly larger than the vertical one. Therefore, waves may break when the horizontal fluid motion exceeds certain value far before the vertical acceleration reaches the breaking criterion. The physical appearances of these two kinds of breaking might, also, be quite different; the fluid separates from the wave in the horizontal direction in one case and in the vertical direction in the other. They both, however, can serve as effective means of restraining the wave growth.

A commonly invoked criterion in the horizontal direction is that the horizontal fluid velocity at the surface exceeds a certain fraction of wave celerity. Again utilizing linear wave theory, this criterion can be expressed as

$$u_p = \frac{A_c(k_o) g k_o}{\sigma_o} = \alpha_1 c \tag{37}$$

where u_p is the horizontal component of water particle velocity, α_1 is a constant and c is the wave celerity. For a monochromatic wave train, one may argue from physical intuition that a wave will break when the horizontal

fluid motion exceeds the wave celerity, or equivalently, α_1 should be equal to unity. Field observation and experimental evidences seem to indicate that α_1 should be around 0.5.

The widely used Miche's (1944) limiting steepness wave in shallow water, for instance, can be shown as equivalent to Eq. (37) with a value of $\alpha_1 = 0.45$. The modified Miche's criterion as used in this work (Eq. 21) will yield a value of $\alpha_1 = 0.38$. It is also interesting to observe here that the criterion expressed in the above equation when applied to deepwater becomes equivalent to the acceleration criterion of Eq. (33), provided $\alpha = \alpha_1$. Longuet-Higgins (1976) recently showed that the wave will break when A_v attains 0.397 g, in other words, $\alpha = 0.397$ which is indeed compatible with the range of values of α_1 indicated here.

If the same procedures used to arrive at the acceleration-limited equilibrium function are followed, the velocity-limited counterpart can be obtained. It assumes the following form:

$$g_u(k) = \left(\frac{\alpha_1}{\gamma}\right)^2 \frac{\tanh kd \,(\tanh kd - kd \,\mathrm{sech}^2 kd)}{k^3} \tag{38}$$

When matched with the deepwater equilibrium condition, the coefficient $\left(\frac{\alpha_1}{\gamma}\right)^2$ is found to be equal to 9.4×10^{-2}.

Like $G_a(k)$, a normalized function $G_u(k)$ can be defined such that

$$G_u(k) = \frac{g_u(k)}{\left(\frac{\alpha_1}{\gamma}\right)^2} \tag{39}$$

Similar to the acceleration-limited equilibrium function, the value of $k^3 g_u(k)$ or $k^3 G_u(k)$, is a function of kd only. This relationship is plotted in the same graph with $k^3 G_a(k)$ in Fig. 30 to offer comparison. In contrast to $k^3 G_u(k)$, the function $k^3 G_u(k)$ is a monotonically increasing function with increasing kd and approaches asymptotically to the constant value as $k^3 G_a(k)$ when $kd \to \infty$.

Field data seemed to support the trend as depicted by the curve $k^3 G_u(k)$. Pierson's data from the stereo-wave observation project (1962) is plotted in the same figure to indicate this trend. In plotting these data, an arbitrary water depth $d = 10$ m was assumed. Thus, the comparison is only qualitative. The variations of $G_u(k)$ with kd is shown in Fig. 31 to offer a comparison with $G_a(k)$. Unlike $G_a(k)$, $G_u(k)$ assumes a bell-shape and has a maximum at $kd \simeq 0.072$. This, at least, offers a possible explanation as to why most of the energy spectra obtained in the field are bell-shaped and have a selected range of wave number or frequency that has a larger energy-containing capacity.

The corresponding equilibrium function in frequency domain based upon velocity criterion, $\phi_u(n)$ can be computed in a similar fashion as $\phi_a(n)$. Unlike $\phi_a(n)$, $\phi_u(n)$ is not an invariant with d when $u = 0$. Examples of $\phi_u(n)$ as function of u with d = constant are plotted in Figs. 32 and 33 with the corresponding $\phi_a(n)$ curves. The variation of $\phi_u(n)$ with d keeping u constant is shown in Figs. 34 and 35 where $\phi(n)$ curves are plotted with the same condition. From these figures, it can be seen that $\phi_u(n)$ and $\phi_a(n)$ intersect at a certain frequency n_p. For wave components of $n > n_p$, the equilibrium is maintained by acceleration criterion. When fluid acceleration exceeds this criterion, breaking occurs with the appearance of spilling

over. For wave components of $n < n_p$, the equilibrium is governed by the horizontal fluid velocity. When fluid velocity exceeds this limit, breaking also occurs with the appearance of curling over, or commonly known as plunging. This composite picture is illustrated in Fig. 36.

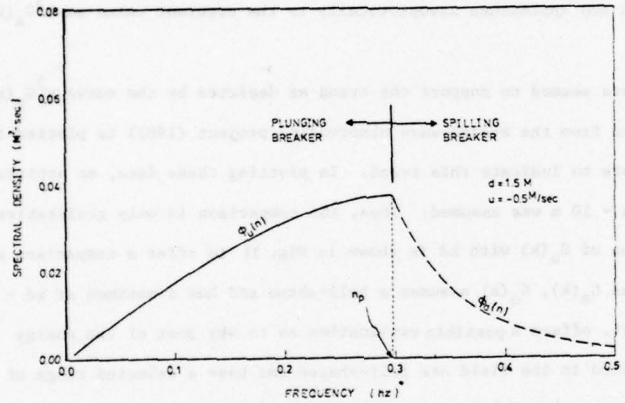

Fig. 36: Composite equilibrium curve of breaking criteria

A number of comparisons between field data and the composite equilibrium curves are shown in Figs. 37 to 38. The cases selected here are either fully breaking or partially breaking waves. The current used in these cases are not actually measured values but arbitrary assigned to yield better comparisons. The range of these values are, however, not unreasonable under the actual conditions.

8. Wave Climate at the Test Site

Based on field observation, aided by the computer prediction, some assessment can be made on the wave climate at the test site. Since the field measurement was conducted for a relatively short period with the highest measured significant wave height up to only 1.5 M neither statistical infor-

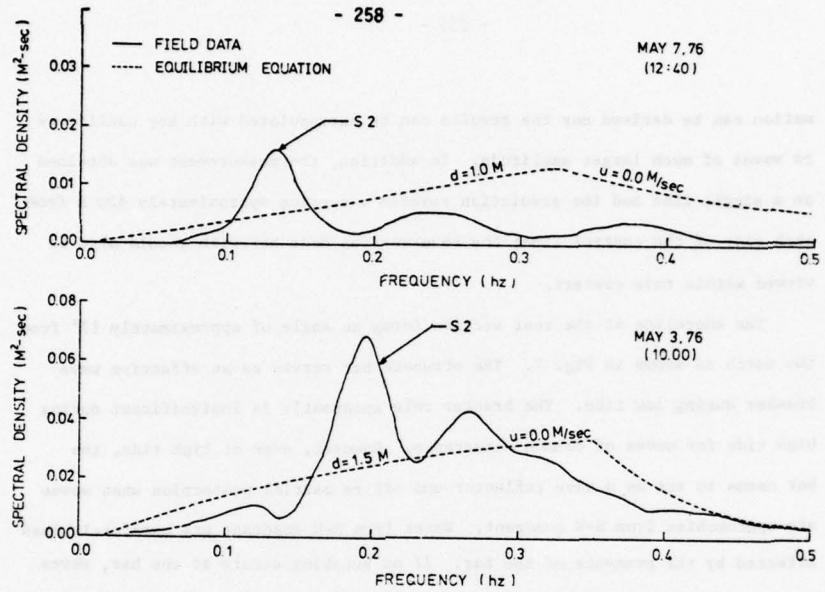

Fig. 37: Comparisons between field data and composite equilibrium curves (Data from May 3 and May 7, 1976)

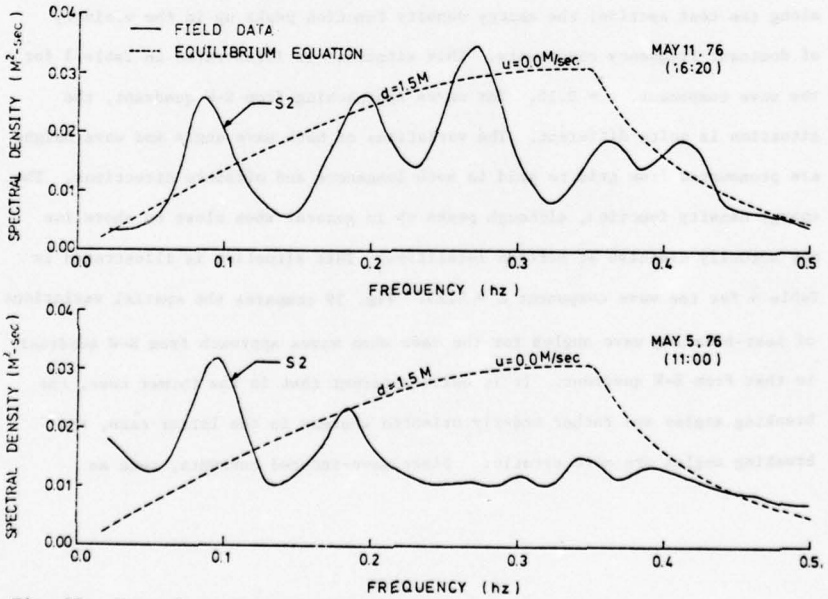

Fig. 38: Comparisons between field data and composite equilibrium curves (Data from May 5 and May 11, 1976)

mation can be derived nor the results can be extrapolated with any confidence to waves of much larger amplitude. In addition, the measurement was obtained on a single line and the prediction covered a section approximately 400 m from each side of the control line; the observations made herewith should also be viewed within this context.

The shoreline at the test section forms an angle of approximately 17° from the north as shown in Fig. 7. The offshore bar serves as an effective wave breaker during low tide. The breaker role apparently is insignificant during high tide for waves of common occurrance. However, even at high tide, the bar seems to act as a wave reflector and offers partial protection when waves are approaching from S-W quadrant. Waves from N-W quadrant are manifestly less affected by the presence of the bar. If no breaking occurs at the bar, waves from the N-W quadrant are, in general, amplified when approaching shoreline; the wave amplification as well as the incident angle appears to be rather uniform along the test section; the energy density function peaks up in the vicinity of dominant frequency components. This situation is illustrated in Table 3 for the wave component, n = 0.15. For waves approaching from S-W quadrant, the situation is quite different. The variations of both wave angle and wave height are pronounced from grid to grid in both longshore and offshore directions. The energy density function, although peaks up in general when close to shoreline may actually diminish at certain localities. This situation is illustrated in Table 4 for the wave component n = 0.15. Fig. 39 compares the spatial variations of near-breaking wave angles for the case when waves approach from N-W quadrant to that from S-W quadrant. It is quite apparent that in the former case, the breaking angles are rather orderly oriented whereas in the latter case, the breaking angles are more erratic. Since wave-induced currents, such as

WAVE APPROACHING ANGLE IN DEGREE

0.000	0.000	0.000	0.000	0.000	0.000	0.000	0.000	0.000	0.000	0.000
0.000	0.000	0.000	0.000	0.000	0.000	0.000	0.000	0.000	0.000	0.000
5.195	5.195	5.650	5.756	5.650	5.756	5.756	5.541	5.429	5.195	4.544
6.587	6.587	13.477	8.680	7.656	6.250	1.933	5.616	10.774	5.059	5.403
7.210	7.210	14.386	8.436	7.336	6.940	2.431	6.276	8.565	3.845	5.988
7.691	7.691	12.719	7.342	7.595	6.741	2.644	5.222	6.402	4.172	6.528
7.336	7.336	10.698	6.926	8.325	5.943	2.965	3.821	6.524	4.841	7.672
6.417	6.417	8.783	6.448	7.914	6.389	4.455	3.954	7.295	5.767	8.234
6.743	6.743	7.208	6.124	7.683	5.956	5.129	6.787	8.375	6.527	8.442
6.158	6.158	6.112	6.366	7.810	6.497	5.995	8.051	7.630	6.032	7.575
6.955	6.955	6.787	6.963	8.612	6.965	6.458	8.199	9.058	7.524	7.763
7.847	7.847	7.642	7.721	8.781	7.789	7.336	8.654	9.393	7.840	8.676
8.408	8.408	8.180	8.112	9.539	8.497	7.872	8.839	9.759	8.756	8.947
8.882	8.882	8.720	8.641	9.768	8.470	8.432	9.093	9.606	9.298	8.790
9.161	9.161	9.272	8.947	9.637	8.909	8.897	9.339	9.551	9.652	8.972
9.375	9.375	9.410	9.224	9.492	9.391	9.382	9.445	9.646	9.700	9.327
9.410	9.410	9.580	9.497	9.593	9.707	9.539	9.566	9.738	9.746	9.752
9.645	9.645	9.749	9.648	9.713	9.716	9.683	9.719	9.789	9.825	9.795
9.756	9.756	9.718	9.756	9.794	9.832	9.868	9.868	9.868	9.868	9.832

WAVE HEIGHT MATRIX

0.000	0.000	0.000	0.000	0.000	0.000	0.000	0.000	0.000	0.000	0.000
0.000	0.000	0.000	0.000	0.000	0.000	0.000	0.000	0.000	0.000	0.000
1.389	1.438	1.456	1.480	1.470	1.505	1.469	1.484	1.496	1.438	1.141
1.219	1.191	1.224	1.263	1.298	1.340	1.280	1.212	1.329	1.372	1.360
1.207	1.174	1.242	1.257	1.248	1.289	1.241	1.226	1.341	1.321	1.311
1.200	1.202	1.287	1.284	1.256	1.293	1.246	1.255	1.308	1.290	1.287
1.190	1.211	1.284	1.285	1.316	1.334	1.260	1.245	1.268	1.233	1.278
1.215	1.216	1.267	1.266	1.291	1.345	1.309	1.238	1.251	1.219	1.220
1.200	1.220	1.259	1.246	1.278	1.300	1.252	1.221	1.241	1.216	1.215
1.228	1.233	1.230	1.225	1.229	1.246	1.233	1.281	1.296	1.252	1.254
1.200	1.202	1.196	1.176	1.201	1.210	1.187	1.182	1.201	1.239	1.235
1.171	1.171	1.167	1.163	1.171	1.168	1.156	1.163	1.176	1.168	1.175
1.159	1.158	1.155	1.145	1.147	1.156	1.140	1.139	1.156	1.152	1.166
1.147	1.150	1.144	1.140	1.150	1.147	1.138	1.134	1.143	1.147	1.145
1.141	1.139	1.140	1.137	1.144	1.141	1.134	1.134	1.135	1.137	1.140
1.136	1.137	1.137	1.135	1.137	1.135	1.134	1.134	1.134	1.136	1.137
1.136	1.135	1.134	1.133	1.133	1.134	1.133	1.132	1.133	1.133	1.134
1.133	1.132	1.133	1.133	1.133	1.133	1.132	1.131	1.132	1.132	1.132
1.132	1.132	1.133	1.132	1.132	1.131	1.131	1.131	1.131	1.131	1.131

NEARSHORE SPECTRAL DENSITY AT HZ= 0.150

0.000	0.000	0.000	0.000	0.000	0.000	0.000	0.000	0.000	0.000	0.000
0.000	0.000	0.000	0.000	0.000	0.000	0.000	0.000	0.000	0.000	0.000
1.507	1.615	1.657	1.712	1.688	1.769	1.687	1.722	1.749	1.615	0.947
1.161	1.108	1.171	1.246	1.317	1.402	1.280	1.148	1.380	1.472	1.446
1.138	1.077	1.206	1.234	1.217	1.298	1.203	1.175	1.405	1.362	1.345
1.124	1.129	1.294	1.288	1.232	1.306	1.213	1.231	1.337	1.303	1.294
1.106	1.145	1.287	1.290	1.353	1.390	1.241	1.211	1.256	1.188	1.187
1.153	1.155	1.254	1.253	1.303	1.414	1.338	1.197	1.223	1.161	1.163
1.124	1.162	1.238	1.212	1.275	1.320	1.225	1.105	1.272	1.155	1.153
1.178	1.187	1.181	1.173	1.181	1.214	1.187	1.281	1.312	1.225	1.228
1.124	1.129	1.118	1.080	1.127	1.144	1.101	1.091	1.126	1.199	1.192
1.072	1.071	1.053	1.057	1.071	1.065	1.043	1.057	1.081	1.055	1.061
1.050	1.048	1.043	1.024	1.027	1.043	1.016	1.014	1.043	1.038	1.041
1.028	1.033	1.023	1.016	1.033	1.027	1.012	1.005	1.021	1.028	1.027
1.016	1.014	1.016	1.010	1.023	1.018	1.005	1.004	1.006	1.010	1.016
1.009	1.010	1.011	1.007	1.011	1.006	1.005	1.004	1.004	1.008	0.999
1.008	1.006	1.005	1.004	1.002	1.005	1.004	1.001	1.003	1.004	1.004
1.003	1.002	1.003	1.002	1.002	1.003	1.001	1.000	1.002	1.002	1.003
1.001	1.001	1.002	1.001	1.000	1.000	0.999	0.999	0.999	0.999	1.001

Table 31 Wave Conditions for Waves from S-W Quadrant (n=0.15)

WAVE APPROACHING ANGLE IN DEGREE

0.000	0.000	0.000	0.000	0.000	0.000	0.000	0.000	0.000	0.000	0.000
0.000	0.000	0.000	-2.008	0.000	-2.008	-2.008	-2.837	-2.837	0.000	0.000
-9.721	-9.721	-10.411	-13.307	-10.411	-16.628	-12.685	-7.457	-4.286	-9.721	-8.756
-14.288	-14.288	-4.412	-16.876	-7.939	-19.591	-16.529	-10.997	-5.674	-17.393	-8.234
-14.900	-14.900	-4.346	-15.616	-10.170	-19.574	-17.713	-10.876	-7.827	-18.515	-9.307
-13.478	-13.478	-5.048	-13.227	-9.810	-17.984	-17.355	-11.652	-10.674	-17.949	-10.005
-13.798	-13.798	-7.375	-12.293	-7.169	-15.234	-16.277	-13.829	-11.874	-18.965	-11.346
-14.596	-14.596	-9.892	-12.666	-8.384	-13.300	-12.736	-14.461	-12.195	-18.175	-12.051
-14.141	-14.141	-11.839	-13.294	-9.231	-14.498	-13.658	-12.642	-12.246	-17.135	-12.650
-14.043	-14.043	-13.938	-13.721	-10.885	-15.354	-13.710	-9.262	-10.235	-14.594	-11.670
-14.488	-14.488	-14.778	-15.422	-11.576	-16.031	-15.398	-12.687	-11.865	-13.596	-12.492
-15.237	-15.237	-15.574	-15.618	-13.280	-17.021	-16.508	-13.761	-12.923	-16.244	-14.158
-15.511	-15.511	-15.882	-16.692	-14.440	-16.800	-17.381	-15.656	-13.967	-16.187	-15.113
-15.693	-15.693	-16.245	-16.753	-14.380	-17.182	-17.131	-16.526	-15.307	-15.878	-16.673
-16.429	-16.429	-16.147	-17.007	-15.241	-16.787	-17.270	-16.639	-16.421	-16.416	-17.139
-16.539	-16.539	-16.369	-16.979	-16.266	-16.832	-16.983	-16.837	-16.576	-16.483	-17.995
-16.824	-16.824	-16.679	-16.976	-16.897	-16.666	-17.028	-17.051	-16.735	-16.765	-16.779
-16.995	-16.995	-16.752	-17.005	-16.898	-16.908	-17.053	-17.117	-17.026	-16.889	-16.873
-16.974	-16.974	-16.911	-16.974	-17.036	-17.097	-17.158	-17.158	-17.158	-17.158	-17.097

WAVE HEIGHT MATRIX

0.000	0.000	0.000	0.000	0.000	0.000	0.000	0.000	0.000	0.000	0.000
0.000	0.000	0.000	0.000	0.000	0.000	0.000	0.000	0.000	0.000	0.000
1.619	1.667	1.715	1.689	1.780	1.974	1.234	1.693	1.873	1.679	1.418
1.463	1.386	1.479	1.448	1.605	1.814	1.199	1.457	1.712	1.573	1.597
1.452	1.392	1.468	1.448	1.544	1.727	1.253	1.466	1.699	1.567	1.556
1.445	1.431	1.505	1.470	1.542	1.695	1.325	1.495	1.650	1.554	1.527
1.436	1.449	1.506	1.469	1.583	1.703	1.388	1.490	1.592	1.539	1.474
1.459	1.465	1.502	1.460	1.548	1.680	1.458	1.483	1.553	1.502	1.464
1.445	1.474	1.506	1.451	1.532	1.619	1.421	1.452	1.522	1.497	1.461
1.471	1.488	1.488	1.442	1.480	1.554	1.421	1.493	1.559	1.529	1.503
1.445	1.456	1.459	1.435	1.447	1.508	1.401	1.480	1.451	1.505	1.487
1.419	1.422	1.426	1.423	1.415	1.455	1.388	1.390	1.424	1.432	1.429
1.408	1.409	1.416	1.391	1.390	1.434	1.388	1.375	1.399	1.417	1.419
1.397	1.406	1.402	1.391	1.393	1.417	1.392	1.380	1.387	1.406	1.402
1.392	1.389	1.395	1.391	1.388	1.405	1.391	1.384	1.384	1.393	1.395
1.389	1.389	1.391	1.391	1.386	1.392	1.390	1.385	1.385	1.391	1.389
1.388	1.387	1.387	1.389	1.385	1.388	1.389	1.386	1.385	1.386	1.388
1.386	1.386	1.386	1.387	1.386	1.387	1.387	1.386	1.385	1.386	1.387
1.386	1.386	1.386	1.386	1.386	1.385	1.385	1.385	1.385	1.385	1.385

NEARSHORE SPECTRAL DENSITY AT HZ= 0.150

0.000	0.000	0.000	0.000	0.000	0.000	0.000	0.000	0.000	0.000	0.000
0.000	0.000	0.000	0.000	0.000	0.000	0.000	0.000	0.000	0.000	0.000
1.365	1.447	1.551	1.349	1.650	2.031	0.793	1.492	1.826	1.468	1.047
1.115	1.000	1.140	1.092	1.241	1.714	0.748	1.115	1.526	1.289	1.326
1.098	1.009	1.123	1.092	1.241	1.554	0.817	1.120	1.503	1.278	1.251
1.088	1.067	1.179	1.125	1.238	1.496	0.915	1.165	1.419	1.258	1.214
1.074	1.093	1.182	1.124	1.305	1.511	1.004	1.157	1.319	1.186	1.132
1.109	1.117	1.175	1.113	1.248	1.470	1.106	1.146	1.256	1.174	1.116
1.088	1.132	1.182	1.097	1.222	1.365	1.051	1.099	1.206	1.167	1.112
1.128	1.153	1.153	1.084	1.142	1.258	1.052	1.161	1.266	1.217	1.177
1.088	1.104	1.108	1.028	1.091	1.185	1.022	1.020	1.096	1.180	1.151
1.048	1.053	1.062	1.025	1.043	1.103	1.004	1.007	1.056	1.067	1.085
1.032	1.034	1.044	1.008	1.006	1.071	1.003	0.985	1.019	1.046	1.048
1.017	1.021	1.024	1.008	1.010	1.045	1.010	0.992	1.002	1.030	1.024
1.009	1.005	1.014	1.007	1.003	1.028	1.008	0.997	0.997	1.011	1.013
1.004	1.004	1.007	1.007	1.000	1.009	1.007	1.000	0.999	1.003	1.004
1.004	1.002	1.002	1.004	0.999	1.004	1.005	1.000	0.999	1.001	1.002
1.001	1.000	1.001	1.002	1.001	1.001	1.002	1.000	0.999	1.000	1.001
1.000	1.000	1.001	1.000	1.000	1.000	0.999	0.999	0.999	0.999	1.000

Table 4: Wave Conditions for Waves from N-W Quadrant (n=0.15)

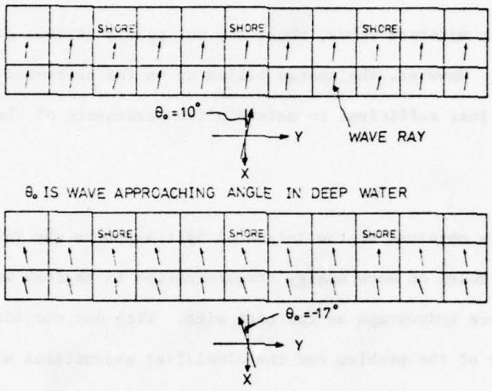

Fig. 39: Comparison of spatial variations of near-breaking wave angles approaching from N-W quadrant to that from S-W quadrant

the longshore drift is governed by wave angle and wave height, one expects that along the test section waves from the N-W quadrant should be more effective in creating an undisrupted longshore current than that from the S-W quadrant. The latter offers a better chance to create circulation cells.

As pointed out, already in previous sections, waves from the S-W are more varied spatially and are more sensitive to the bottom changes. This point is well illustrated in Fig. 29 where the predicted spectrum at 75 m (the adjacent grid) south of station 2 is compared with that at Station 2; the change is quite significant for two adjacent grids.

Although the offshore bar plays a protection role most of the time, it also could occasionally become an energy trapper to prevent wave energy from escaping the inshore zone. This occurs mainly under the offshore wind condition as shown in Fig. 13. Fortunately, this condition often

is associated with moderate waves, thus, may not pose a serious condition to shore erosion. However, the energy piling up on the shoreward side of the bar might be just sufficient to maintain the permanence of the bar.

9. Conclusions

The field data obtained at the Island of Sylt supports the validity of the numerical model on wave energy transformation in regions with as complex a nearshore hydrograph as the test site. With due consideration on the complexity of the problem and the simplified assumptions made in the modeling, the numerical predictions yield quite acceptable results of energy-containing wave components and long-wave components. In these ranges, the agreement between predicted results and field data is considered good up and prior to breaking. It suggests that the transformation of waves components within these ranges is mainly influenced by shoaling and refraction, the two factors included in the modeling. The numerical results are unsatisfying in high frequency components where local effects of energy dissipation, generation or transfer are deemed to be more important. All these effects are not being considered in the present model.

Turbulent generation due to wave instability seems to be the dominant mechanism of energy dissipation as opposed to bottom friction which seems to play a very minor role except in the region of wave uprush. Based upon commonly used wave instability criteria, the equilibrium energy spectral density function in shoaling water has been developed. This function provides saturation condition on spectral density for the complete frequency (or wave-number) range and, thus, enables one to estimate the limiting

spectra as functions of local water depth and current conditions. Comparisons with field data are encouraging, in particular, for cases where waves break over offshore obstacles such as the offshore bar in the present study. An explanation has been offered on the difference between spilling and plunging breakers.

The limited field data alone does not provide sufficient information to perform wave climate assessment at the test location. However, when coupled with numerical computations which extend the point information to spatial distribution certain general observations can be made. The offshore bar plays the double roles as energy dissipator and trapper depending mainly on the wind direction,tidal stage and wave height. For low tide, the role of dissipation dominates. For high tide and nonbreaking wave, the bar acts like a partial reflector under onshore wind and an energy trapper under offshore wind. Waves fron the N-W quadrant are found to be less affected by the bar and are more effective in generating unidirectional longshore drift directing southward. Waves from the S-W quadrant appear to have greater spatial variations both in wave angle and wave magnitude and are likely to promote nearshore circulation cell. For wind wave conditions, the JONSWAP spectra are reasonable deepwater inputs for the tested region. All the above observations await further field experiment for verification.

In conclusion, the numerical model has shown to be valid and provides a sueful tool to yield spatial information on wave energy spectra in nearshore zone. Further improvements could be made in the following directions:

1. Field data with simultaneous current information.
2. The effect of directional spreading.
3. The interaction among wave components

and in that order of importance. Analytical and experimental work should be continued in the area of developing limiting wave spectra in shallow water. This information should be useful in determining limiting design condition for engineering purposes.

10. References

Blackman, R.B., and J.W. Tukey, The Measurement of Power Spectra, Dover Publications, New York, 1958.

Büsching, F., Über die Änderung von Wellenperioden im Brandungsbereich, Sonderdruck aus Heft 47 der Mitteilungen des Leichtweiß- Instituts für Wasserbau der Technischen Universität Braunschweig, 1975.

Collins, J.I., Prediction of Shallow-Water Spectra, J. of Geophys. Res., Vol. 77, No. 15, May, 1972, pp. 2693-2707.

Colley, J.W. and Tukey, J.W., An Algorithm for the Machine Calculation of Complex Fourier Series, Math. of Computation, V. 19(99), pp. 297-301, 1965.

Divoky, D., et al., Breaking Waves on Gentle Slopes, J. of Geophys. Res., Vol. 75, No. 9, March 20, 1970, pp. 1681-1692.

Fahrentholz, S.R., Waves and Sea-Level Measurements in the Open Sea by Use of Echo-Sounding Methods, Laboratorium der Firma Dr. Fahrentholz, Echolote und Elektronik, in Kiel (BRD) (I 0 73-657).

Führböter, A. and F. Büsching, Wave Measuring Instrumentation for Field Investigations on Breakers, Proceedings of the International Symposium on Ocean Wave Measurement and Analysis, New Orleans, Sept., 1974.

Hasselmann, K., et al., Measurements of Wind-Wave Growth and Swell Decay During the Joint North Sea Wave Project (JONSWAP), Deutsches Hydrographisches Institut, Hamburg, 1973.

Karlesson, T., Refraction of Continuous Ocean Wave Spectra, J. of Waterways, Harbors and Coastal Engrg. Div., ASCE, WW4, Nov., 1969, pp. 437-448.

Krasitskiy, V.P., Toward a Theory of Transformation of the Spectrum on Refraction of Wind Waves, Izv. Atmospheric and Oceanic Physics, Vol. 10, No. 1, 1974, pp. 72-82.

Longuet-Higgins, M.S., The Refraction of Sea Waves in Shallow Water, J.F.M., Vol. 1, Part 2, 1956, pp. 163-176.

Longuet-Higgins, M.S. and R.W. Stewart, Changes in the Form of Short Gravity Waves on Long Waves and Tidal Currents, J. Fluid Mech. 8, 1960, pp. 565-583.

Longuet-Higgins, M.S. and R.W. Stewart, The Changes in Amplitude of Short Gravity Waves on Steady Non-Uniform Currents, J. Fluid Mech., 10, 1961, pp. 529-549.

Longuet-Higgins, M.S., E.D. Cokelet, The Calculation of Steep Gravity Waves, Proceedings, Behavior of Offshore Structures, Norwegian Inst. of Technology, Trondheim, 1976, Vol. 2.

Miche, M., Mouvements Ondulatoires de la Mer en Profondeur Constante ou Decroissante, Annales des Ponts et Chaussees, 1944.

Noda, E., et al., Nearshore Circulations Under Sea Breeze Conditions and Wave-Current Interactions in the Surf Zone, Tetra Tech, Report TC-149-4, Feb., 1974.

Phillips, O.M., The Equilibrium Range in the Spectrum of Wind-Generated Waves, J. Fluid Mech., 4, 1958, pp. 426-434.

Phillips, O.M., The Dynamics of the Upper Ocean, Cambridge University Press, 1966.

Pierson, W.J. (ed), The Directional Spectrum of a Wind Generated Sea as Determined from Data Obtained by the Stereo Wave Observation Project, College Engrg., N.Y.U., Met. Paper 2, 1962, No. 6.

Pierson, W.J., Jr. and L. Moskowitz, A Proposed Spectral Form for Fully Developed Wind Seas Based on the Similarity Theory of S.A. Kitaigorodskii, J. Geophys. Res., 1969.

Shiau, J.C. and Wang, H., Wave Energy Transformation Over Irregular Bottom, J. Waterway, Harbor and Coastal Engrg., ASCE, 1976 (in press).

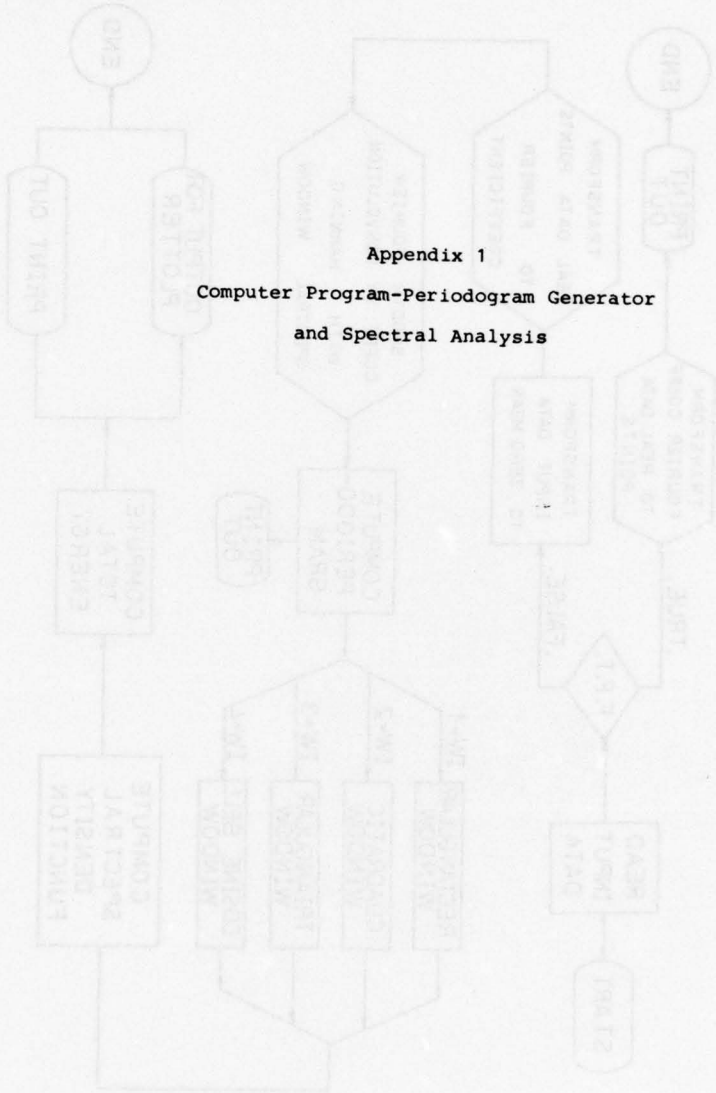

Appendix 1

Computer Program-Periodogram Generator

and Spectral Analysis

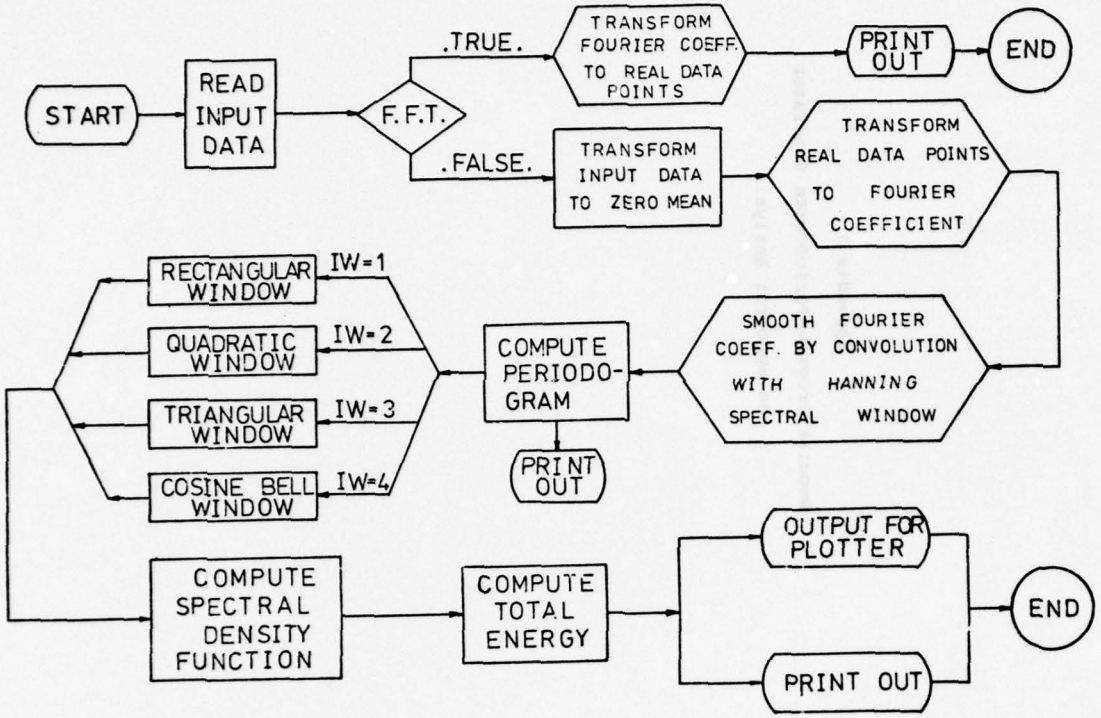
START
READ INPUT DATA
F.F.T.
.TRUE.
TRANSFORM FOURIER COEFF. TO REAL DATA POINTS
PRINT OUT
END
.FALSE.
TRANSFORM INPUT DATA TO ZERO MEAN
TRANSFORM REAL DATA POINTS TO FOURIER COEFFICIENT
SMOOTH FOURIER COEFF. BY CONVOLUTION WITH HANNING SPECTRAL WINDOW
COMPUTE PERIODO-GRAM
PRINT OUT
RECTANGULAR WINDOW
IW=1
QUADRATIC WINDOW
IW=2
TRIANGULAR WINDOW
IW=3
COSINE BELL WINDOW
IW=4
COMPUTE SPECTRAL DENSITY FUNCTION
COMPUTE TOTAL ENERGY
OUTPUT FOR PLOTTER
PRINT OUT
END

```
      MASTER MAIN
C     PURPOSE--PERIODOGRAM GENERATOR AND SPECTRAL ANALYSIS
C     INPUT ARRANGEMENTS--
C     N1,.....,N8 ARE WAVE DATA INDEXEX OF THE FILE
C     NPTS IS THE TOTAL NUMBER OF REAL DATA VALUES CONTAINED
C     IN X(I)
C     NOTE--NPTS MUST BE 2**(M1/2),M1.GE.4
C     NAV IS THE AVERAGE VALUE OF X(I)
C     NCA IS THE CALIBRATION VALUE OF X(I)
C     NEWDEG IS THE DEGREE OF FREEDOM USED IN SPECTRAL ANALYSIS
C     NEWWIN IS ONE OF THE WINDOW(1-4) USED TO SMOOTH PERIODOGRAM
C     IZ(I) IS DUMMY ARRAY
C     DELT IS THE TIME INCREMENT BETWEEN X(I) AND X(I+1)
C     FREQMX IS THE MAXIMUM FREQUENCY DESIRED TO PRINT OUT
C
      DIMENSION IX(8192),IZ(8192),X(4097),Y(4097)
      DIMENSION A(4097),B(4097),ILST(88)
      COMMON/B1/S(4097),SBAR(4097),DELF,NP
C     READ BASIC DATA
C     READ DATA INDEX
      READ (5,5030) N1,N2,N3,N4,N5,N6,N7,N8
      READ (5,5010) NPTS,NCA,NEWDEG,NEWWIN
      READ (5,5020) DELT,FREQMX
C     READ WAVE DATA
      READ (5,5030) (IZ(I),IX(I),I=1,NPTS)
      WRITE (6,6000) N1,N2,N3,N4,N5,N6,N7,N8
      WRITE (6,6005) NPTS,NEWDEG,NEWWIN
C     TRANSFORMATION OF DATA POINTS TO ZERO MEAN VALUE
      ISUMX=0
      DO 99 I=1,NPTS
99    ISUMX=IX(I) +ISUMX
C     AVX IS AVERAGE VALUE OF IX(I)
      AVX=FLOAT(ISUMX/NPTS)
      DO 100 I=1,NPTS
      X(I)=(FLOAT(IX(I))-AVX)/NCA
```

```
100   CONTINUE
C     ZERO MEAN REAL DATA POINTS STORED IN
C     X(1),.....,X(NPTS)
      NPTS2=NPTS/2
      N1=NPTS2+1
      M1=2*INT(ALOG2(FLOAT(NPTS)))
      DO 101 I=1,NPTS2
      A(I)=X(I)
      B(I)=X(I+NPTS2)
101   CONTINUE
      NP=(NPTS*2)/2
      CALL C06AAF (A,B,N1,.FALSE.,M1,ILST)
      CALL HANN (A,B,NPTS,NPTS2)
      DO 102 I=1,NPTS2
      S(I)=(A(I)**2+B(I)**2)*(NPTS*DELT)/2.
102   CONTINUE
C     PERIODOGRAM STORED IN S(1),.....,S(NPTS2)
      WRITE (6,601)
      WRITE (6,602) (S(I),I=1,NPTS2)
      DELF=1.0/(NPTS*DELT)

      CALL SMOOTH(NEWDEG,NEWDIM,3W)
      NPTSPT=INT(FREQMX/DELF)+1
      TATENG=0.0
      DO 620 I=1,NPTSPT
      X(I)=DELF*(I-1)
      Y(I)=SBAR(I)
      TATENG=TATENG+Y(I)
620   CONTINUE
C     FINAL RESULT OF FREQUENCY X(I) AND CORRESPONDING
C     SPECTRAL DENSITY Y(I)
      TATENG=TATENG*DELF*(2.*3.1415926535)
      WRITE (6,603) TATENG
      WRITE (6,603)
      WRITE (6,604)
      WRITE (6,602) (X(I),Y(I),I=1,NPTSPT)
```

```
5010  FORMAT (5(I6,2X))
5020  FORMAT (2(F5.2,2X))
5030  FORMAT (8(I5,2X))
5040  FORMAT (//,1X,'WAVE INDEX=',8I6)
5050  FORMAT (//,1X,'TOTAL DATA POINTS =',I5,
     1'   DEGREE OF FREEDOM=',I3,'   SPECTRAL WINDOW=',I2)
5010  FORMAT (//,1X,'THE PERIODOGRAM FROM X(1) TO X(NP) IS')
5020  FORMAT (8F8.3)
5030  FORMAT (//,1X,'OUTPUT OF FREQUENCY X(I) AND',1X,
     1'CORRESPONDING SPECTRAL DENSITY Y(I)')
5040  FORMAT (//,2X,'X(I)',3(4X,'Y(I)',4X,'X(I)'),4X,'Y(I)')
5050  FORMAT (//,1X,'TOTAL WAVE ENERGY =',F8.5)
      STOP
      END


      SUBROUTINE HANN(A,B,NPTS,NPTS2)
C     PURPOSE--SMOOTH THE RAW FOURIER COEFFICIENTS BY CONVOLUTION
C     WITH THE HANNING SPECTRAL WINDOW
C     INPUT ARRANGEMENTS--
C     NPTS IS THE TOTAL NUMBER OF COMPLEX COEFFICIENTS CONTAINED
C     IN X(I)
C
      DIMENSION A(4097),B(4097)
      STORE=A(1)
      A(1)=0.5*(STORE+A(2))
      DO 10 I=2,NPTS2
      TEMP=A(I)
      A(I)=0.25*(STORE+A(I+1))+0.5*TEMP
      STORE=TEMP
10    CONTINUE

      STORE=B(1)
      B(1)=0.5*(STORE+B(2))
      DO 20 I=2,NPTS2
```

```
      TEMP=B(I)
      B(I)=0.25*(STORE+B(I+1))+0.5*TEMP
      STORE=TEMP
20    CONTINUE
      RETURN
      END

      SUBROUTINE SMOOTH(NU,IW,BW)
C     PURPOSE--AVERAGE THE RAW PERIODOGRAM STORED IN ARRAY S(I)
C     TO OBTAIN SEPARATE ARRAY SBAR(J) OF SMOOTHED SPECTRAL
C     ELEMENTS

C     THE AVERAGING IS ACCOMPLISHED BY CONVOLUTING A SERIES OF
C     WEIGHTING COEFFICIENTS W(I), TERMED A SPECTRAL WINDOW,
C     WITH THE PERIODOGRAM
C     NU=NEWDEG   IW=NEWWIN
C     BW SPECIFIES THE BANDWIDTH RESOLUTION OF THE SMOOTHED
C     ESTIMATES
C
      COMMON/B1/S(4097),SBAR(4097),DELF,NP
      REAL A(4)/0.25,0.30,0.333,0.375/,PI/3.14159265358/,
     1     W(61)/61*0.0/
      BW=DELF*NU/2.
C     NUMBER OF WEIGHTING COEFFICIENTS EQUALS 2*M+1
      M=INT((2.*NU*A(IW)-1.)/2.)
      SUM=0.
      IF (M.LT.1) GO TO 50
C     COMPUTING WEIGHTING COEFFICIENTS W(I)
      IF (IW-3) 10,40,50
10    IF (IW-1) 20,20,30
C     WHEN IW=1,USE RECTANGULAR WINDOW
20    DO 25 I=1,M
      W(I+1)=1./(2.*M+1.)
```

```
      SUM=SUM+W(I+1)
25    CONTINUE
      GO TO 60

C     WHEN IW=2,USE QUADRATIC WINDOW
30    DO 35 I=1,M
      W(I+1)=(1.5/(2.*M+1.))*(1.-(2.*I/(2.*M+1.))**2)
      SUM=SUM+W(I+1)
35    CONTINUE
      GO TO 60
C     WHEN IW=3, USE TRIANGULAR WINDOW
40    DO 45 I=1,M
      W(I+1)=(2./(2.*M+1.))*(1.-(2.*I/(2.*M+1.)))
      SUM=SUM+W(I+1)
45    CONTINUE
      GO TO 60
C     WHEN IW=4, USE COSINE BELL WINDOW
50    DO 55 I=1,M
      W(I+1)=(1./(2.*M+1.))*(1.+COS(2.*PI*I/(2.*M+1.)))
      SUM=SUM+W(I+1)
55    CONTINUE
60    W(1)=1.-2.*SUM
C     CONVOLUTE WEIGHTING COEFFICIENTS WITH PERIODOGRAM
C     STORE RESULT IN SBAR(I)
      DO 80 I=1,NP
      SUM=0.0
      DO 70 J=1,M
      IPLUSJ=I+J
      IF(IPLUSJ.GT.NP) IPLUSJ=NP-(IPLUSJ-NP)
      IMNUSJ=I-J
      IF(IMNUSJ.LT.1) IMNUSJ=IABS(IMNUSJ)+2
      SUM=SUM+W(J+1)*(S(IPLUSJ)+S(IMNUSJ))
70    CONTINUE
      SBAR(I)=SUM+W(1)*S(I)
80    CONTINUE
      RETURN
      END
```

```
      SUBROUTINE C06AAF(A,B,N1,INVERS,M1,ILST)
C     MARK 2 RELEASE. NAG COPYRIGHT 1972
C     MARK 3 REVISED.
      LOGICAL INVERS
      DIMENSION A(N1),B(N1),ILST(M1)
C     COMPUTES F.F.T. OF 2*N=2**(M+1) REAL DATA POINTS
C     CONTAINED IN A(1)--A(N),B(1)--B(N) IF INVERS IS
C     .FALSE.
C     N1=N+1,M1=2*(M+1) AND ILST IS A WORK ARRAY 1--M1
      M=M1/2-1
      N=N1-1
      IF(.NOT.INVERS) GO TO 3
      CALL C06AAZ(A,B,N1,.TRUE.)
      DO 1 J=1,N
      B(J)=-B(J)
1     CONTINUE
      CALL C06AAY(A,B,N,M,N)
      DO 2 J=1,N
      A(J)=0.5*A(J)
      B(J)=-0.5*B(J)
2     CONTINUE
      CALL C06AAJ(A,B,N,M,.TRUE.,M1,ILST)
      A(N1)=0.0
      B(N1)=0.0
      GO TO 5
3     CONTINUE
      CALL C06AAN(A,B,N,M,.TRUE.,M1,ILST)
      CALL C06AAX(A,B,N,M,1)
      X1=N
      P=0.5/X1
      DO 4 J=1,N
      A(J)=P*A(J)
      B(J)=P*B(J)
4     CONTINUE
      CALL C06AAZ(A,B,N1,.FALSE.)
```

```
      CONTINUE
      RETURN
      END


      SUBROUTINE C06AAW(A,B,N,KS,REEL,M1,ILST)
C     MARK 2 RELEASE. NAG COPYRIGHT 1972
C     MARK 5 REVISED.
      LOGICAL REEL
      DIMENSION A(N),B(N),ILST(M1)
C     M1=2(M+1) AND ILST IS A WORKING ARRAY 1 TO M1
      M=M1/2-1
      MOR=M
      ILST(M1)=KS
      DO 1 I=1,M
      INDEX=M1-I
1     ILST(INDEX)=ILST(INDEX+1)/2
      IP=M-1
      J=N-1
      I=1
      KB=1
      IF(.NOT.REEL) GO TO 3
      KB=N-1
      DO 2 K=1,KB,2
      T=A(K+1)
      A(K+1)=B(K)
      B(K)=T
2     CONTINUE
      GO TO 4
3     M=N-1
4     IF(IP.LE.0) GO TO 10
      LIM=(M+2)/2
5     INDEX=MOR+2+J
      KU=ILST(INDEX)+KB
      K2=KU
      INDEX=MOR+2+M-J
```

```
      JJ=ILST(INDEX)
      KK=KB+JJ
    6 K=KK+JJ
    7 T=A(KK)
      A(KK)=A(K2)
      A(K2)=T
      T=B(KK)
      B(KK)=B(K2)
      B(K2)=T
      KK=KK+1
      K2=K2+1
      IF(KK.LT.K) GO TO 7
      KK=KK+JJ
      K2=K2+JJ
      IF(KK.LT.KB) GO TO 6
      IF(J.LE.LIM) GO TO 8
      J=J-1
      I=I+1
      ILST(I)=J
      GO TO 5
    8 CONTINUE
      KB=K2
      IF(I.LE.1) GO TO 9
      J=ILST(I)
      I=I-1
      GO TO 5
    9 CONTINUE
      IF(KB.GT.N) GO TO 10
      J=IP
      GO TO 5
   10 CONTINUE
      RETURN
      END
```

```
      SUBROUTINE C06AAX(A,B,N,M,KS)
C     MARK 2 RELEASE. NAG COPYRIGHT 1972
C     MARK 3 REVISED.
      DIMENSION A(N),B(N)
      RAD=4.0*ATAN(1.0)
      MOR=M
      NOR=N
      NOR=NOR-1
      K0=1
      ISPAN=KS
C     IF M IS ODD THEN COMPUTE FOR ONE FACTOR OF 2
      IF((MOR/2)*2-MOR) 1,2,1
1     K2=K0+ISPAN
      A0=A(K2)
      B0=B(K2)
      A(K2)=A(K0)-A0
      A(K0)=A(K0)+A0
      B(K2)=B(K0)-B0
      B(K0)=B(K0)+B0
      K0=K2+ISPAN
      IF(K0.LE.NOR) GO TO 1
      K0=K0-NOR
      IF(K0.NE.ISPAN+1) GO TO 1
      ISPAN=2*ISPAN
      RAD=0.5*RAD
2     CONTINUE
3     MOR=NOR-2
      IF(MOR.LT.0) GO TO 3
      C1=1.0
      C2=1.0
      C3=1.0
      S1=0.0
      S2=0.0
      S3=0.0
      K0=1
```

```
      RAD=0.25*RAD
      DC=2.0*SIN(RAD)**2
      DS=SIN(RAD*RAD)
      K=KS
4     K1=K0+ISPAN
      K2=K1+ISPAN
      K3=K2+ISPAN
      A0=A(K0)
      B0=B(K0)
      IF(S1.NE.0.0) GO TO 5
      A2=A(K1)
      B2=B(K1)
      A1=A(K2)
      B1=B(K2)
      A3=A(K3)
      B3=B(K3)
      GO TO 6
5     CONTINUE
C     THIS IS THE SAME AS THE ABOVE IF SI=0 AND CI=0
      AK=A(K1)
      BK=B(K1)
      A2=AK*C2-BK*S2
      B2=AK*S2+BK*C2
      AK=A(K2)
      BK=B(K2)
      A1=AK*C1-BK*S1
      B1=AK*S1+BK*C1
      AK=A(K3)
      BK=B(K3)
      A3=AK*C3-BK*S3
      B3=AK*S3+BK*C3
6     CONTINUE
      A(K0)=A0+A2+A1+A3
      B(K0)=B0+B2+B1+B3
      A(K1)=A0-A2-B1+B3
      B(K1)=B0-B2+A1-A3
```

```
      A(K2)=A0+A2-A1-A3
      B(K2)=B0+B2-B1-B3
      A(K3)=A0-A2+B1-B3
      B(K3)=B0-B2-A1+A3
      K0=K3+ISPAN
      IF(K0.LE.NOR) GO TO 4
      K0=K0-NOR
      IF(K0.NE.K+1) GO TO 4
C     IF COMPUTING THE CURRENT FACTOR OF 4 IS NOT FINISHED
C     THEN INCREMENT THE SINE COSINE VALUES
      IF(K0.EQ.ISPAN+1) GO TO 7
      C2=C1-(DC*C1+DS*S1)
      S1=(DS*C1-DC*S1)+S1
      C1=C2
      C2=C1**2-S1**2
      S2=2.0*C1*S1
      C3=C2*C1-S2*S1
      S3=C2*S1+S2*C1
      K=K+KS
      GO TO 4
7     CONTINUE
      ISPAN=4*ISPAN
      GO TO 3
8     CONTINUE
      RETURN
      END
      SUBROUTINE C06AAY(A,B,N,M,KS)
C     MARK 2 RELEASE. NAG COPYRIGHT 1972
C     MARK 3 REVISED
      DIMENSION A(N),B(N)
C     COMPUTES THE F.F.T. FOR ONE VALUABLE OF DIMENSION 2**M
C     IN A MULTIVARIATE TRANSFORM OF N DATA POINTS FOR A
C     VARIATE TRANSFORM
C     N=N1*N2*....*NP AND KS=NK*....NP,WHERE NK=2**M IS THE
C     CURRENT VARIATE
      NOR=M
```

```
      NOR=N
      KSOR=KS
      ISPAN=KSOR
      RAD=3.14159265359/X1
      KSOR=ISPAN/KSOR
      NOR=NOR-1
      K=NOR
11    NOR=NOR-2
      IF(NOR.LT.0) GO TO 6
      C1=1.0
      S1=0.0
      S2=0.0
      S3=0.0
      C2=1.0
      C3=1.0
      K0=1
      K=KSOR
      DC=2.0*SIN(RAD)**2
      RAD=2.0*RAD
      DS=SIN(RAD)
      RAD=2.0*RAD
      ISPAN=ISPAN/4
1     K1=K0+ISPAN
      K2=K1+ISPAN
      K3=K2+ISPAN
      A0=A(K0)
      B0=B(K0)
      A1=A(K1)
      B1=B(K1)
      A2=A(K2)
      B2=B(K2)
      A3=A(K3)
      B3=B(K3)
      A(K0)=A0+A2+A1+A3
      B(K0)=B0+B2+B1+B3
      IF(S1) 3,4,3
```

```
2       A(K1)=A0+A2-A1-A3
        B(K1)=B0+B2-B1-B3
        A(K2)=A0-A2-B1+B3
        B(K2)=B0-B2+A1-A3
        A(K3)=A0-A2+B1-B3
        B(K3)=B0-B2-A1+A3
        GO TO 4
C       THIS IS THE SAME AS ABOVE IF CI=0 AND SI=0
3       RE=A0+A2-A1-A3
        RIM=B0+B2-B1-B3
        A(K1)=RE*C2-RIM*S2
        B(K1)=RE*S2+RIM*C2
        RE=A0-A2-B1+B3
        RIM=B0-B2+A1-A3
        A(K2)=RE*C1-RIM*S1
        B(K2)=RE*S1+RIM*C1
        RE=A0-A2+B1-B3
        RIM=B0-B2-A1+A3
        A(K3)=RE*C3-RIM*S3
        B(K3)=RE*S3+RIM*C3
4       K0=K3+ISPAN
        IF(K0.LE.NOR) GO TO 1
        K0=K0-NOR
        IF(K0.NE.K+1) GO TO 1
C       IF COMPUTING FOR THE CURRENT FACTOR OF 4 IS NOT
C       FINISHED THEN INCREMENT THE SINE AND COSINE VALUES
        IF(K0.EQ.ISPAN+1) GO TO 5
        C2=C1-(DC*C1+DS*S1)
        S1=(DS*C1-DC*S1)+S1
        C1=C2
        C2=C1**2-S1**2
        S2=2.0*C1*S1
        C3=C2*C1-S2*S1
        S3=C2*S1+S2*C1
        K=K+KSOR
        GO TO 1
```

```
      5     K=NOR
            GO TO 11
      6     CONTINUE
      C     IF M IS ODD THEN COMPUTE FOR ONE FACTOR OF 2
            IF(K.EQ.0) GO TO 8
            ISPAN=ISPAN/2
            K0=1
      7     K2=K0+ISPAN
            A0=A(K2)
            B0=B(K2)
            A(K2)=A(K0)-A0
            A(K0)=A(K0)+A0
            B(K2)=B(K0)-B0
            B(K0)=B(K0)+B0
            K0=K2+ISPAN
            IF(K0.LE.NOR) GO TO 7
            K0=K0-NOR
            IF(K0.NE.ISPAN+1) GO TO 7
      8     CONTINUE
            RETURN
            END


            SUBROUTINE C06AAZ(A,B,N1,EVAL)
      C     MARK 2 RELEASE. NAG COPYRIGHT 1972
      C     MARK 3 REVISED
            LOGICAL EVAL
            DIMENSION A(N1),B(N1)
      C     N1=N+1
            N=N1-1
            NH=N/2
            X1=N
            R=3.14159265359/X1
            DS=SIN(R)
            R=-(2.0*SIN(0.5*R))**2
            DC=-0.5*R
```

```
      CK=1.0
      SK=0.0
      IF(.NOT.EVAL) GO TO 1
      CK=-1.0
      DC=-DC
      GO TO 2
1     A(N1)=A(1)
      B(N1)=B1
2     NH1=NH+1
      DO 3 K=1,NH1
      NK=N1-K+1
      AA=A(K)+A(NK)
      AB=A(K)-A(NK)
      BA=B(K)+B(NK)
      BB=B(K)-B(NK)
      RE=CK*BA+SK*AB
      RIM=SK*BA-CK*AB
      B(NK)=RIM-BB
      B(K)=RIM+BB
      A(NK)=AA-RE
      A(K)=AA+RE
      DC=R*CK+DC
      CK=CK+DC
      DS=R*SK+DS
      SK=SK+DS
3     CONTINUE
      RETURN
      END
```

Appendix 2

Computer Program-Spectral Transformation Over Irregular Bottom Topography

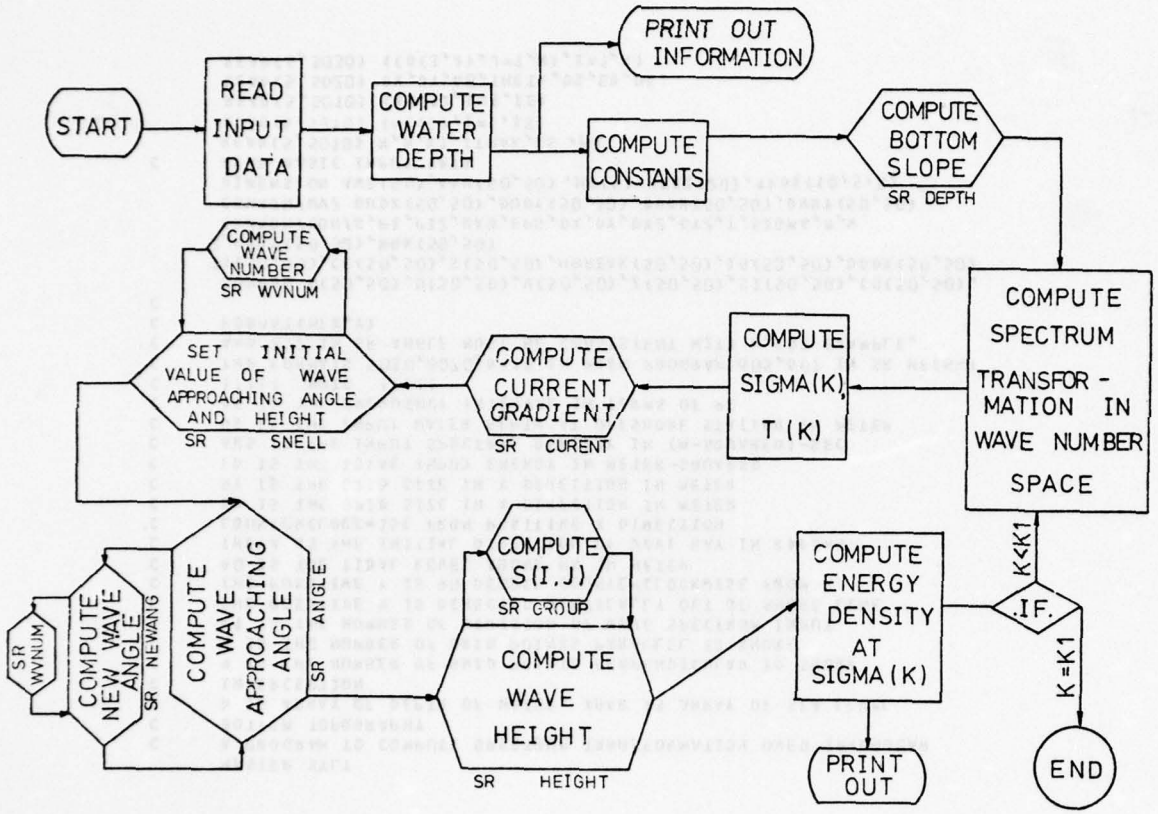
START
READ INPUT DATA
COMPUTE WATER DEPTH
PRINT OUT INFORMATION
COMPUTE CONSTANTS
COMPUTE BOTTOM SLOPE
SR DEPTH
COMPUTE WAVE NUMBER
SR WVNUM
SET INITIAL VALUE OF WAVE APPROACHING ANGLE AND HEIGHT
SR SNELL
COMPUTE CURRENT GRADIENT
SR CURENT
COMPUTE SIGMA(K), T(K)
COMPUTE SPECTRUM TRANSFOR-MATION IN WAVE NUMBER SPACE
K<K1
.IF.
K=K1
END
COMPUTE ENERGY DENSITY AT SIGMA(K)
PRINT OUT
COMPUTE S(I,J)
SR GROUP
COMPUTE WAVE HEIGHT
SR HEIGHT
COMPUTE WAVE APPROACHING ANGLE
SR ANGLE
COMPUTE NEW WAVE ANGLE
SR NEWANG
SR WVNUM

```
      MASTER SYLT
C     A PROGRAM TO COMPUTE SPECTRUM TRANSFORMATION OVER IRREGULAR
C     BOTTOM TOPOGRAPHY
C     D IS ARRAY OF DEPTH OF WATER, XBAR IS ARRAY OF SEA LEVEL
C     INTERCEPTION
C     M IS THE NUMBER OF GRID POINTS PERPENDICULAR TO SHORE
C     N IS THE NUMBER OF GRID POINTS PARALLEL TO SHORE
C     K1 IS THE NUMBER OF DIVISION OF WAVE SPECTRUM INPUT
C     THE POSITIVE X IS DIRECTED VERTICALLY OUT OF SHORE LINE
C     THE POSITIVE Y IS 90 DEGREE COUNTERCLOCKWISE FROM X
C     AO IS THE TIDAL LEVEL ABOVE NN IN METER
C     THETA IS THE INITIAL DIRECTION OF WAVE RAY IN RADIAN
C     COUNTERCLOCKWISE FROM POSITIVE X DIRECTION
C     DX IS THE GRID SIZE IN X DIRECTION IN METER
C     DY IS THE GRID SIZE IN Y DIRECTION IN METER
C     ED IS THE TOTAL INPUT ENERGY IN METER-SQUARED
C     AWS IS THE INPUT SPECTRAL DENSITY IN (M-SQUARED)-SEC
C     DS IS THE INPUT WATER DEPTH AT OFFSHORE STATION IN METER
C     DF IS THE FREQUENCY INTERVAL IN TERMS OF PI
C     !!!!!  NOTE  !!!!!
C     THE FORMATS 5030,6070,6110 IN MAIN PROGRAM;605,607 IN SR HEIGHT
C     AND 252 IN SR ANGLE MUST BE CONSISTENT WITH N,FOR EXAMPLE,
C     FORMAT(NFX.Y)
C
      COMMON D(50,50),U(50,50),V(50,50),Z(50,50),SI(50,50),CO(50,50),
     1H(50,50),CG(50,50),S(50,50),HBREAK(50,50),IB(50,50),DDDX(50,50)
     2,DDDY(50,50),RRK(50,50)
      COMMON/CON/G,PI,PI2,RAD,EPS,DX,DY,DX2,DY2,T,SIGMA,M,N
      COMMON/UV/ DUDX(50,50),DUDY(50,50),DVDX(50,50),DVDY(50,50)
      DIMENSION AWS(50),AAW(50,50),MK(5),HERZ(20),SPDE(10,5,5)
C     READ BASIC INPUT DATA
      READ(5,5010) M,N,K1,ITMAX,IS ,NK
      READ(5,5010) (HK(I),I=1,IS)
      READ(5,5010) (MK(I),I=1,IS)
      READ(5,5020) DX,DY,AO,THETA,DS,ED,DF
      READ(5,5030) ((D(I,J),J=1,N),I=1,M)
```

```
      READ(5,5040) (AWS(I),I=1,K1)
      WRITE(6,6010) M,N,K1,ITMAX
      WRITE(6,6020) DS
      WRITE(6,6030) DX,DY
      WRITE(6,6040) A0
      WRITE(6,6050) THETA
      DO 10 I=1,M
      DO 10 J=1,N
   10 D(I,J)=D(I,J)+A0
      WRITE(6,6060)
      WRITE(6,6070) ((D(I,J),J=1,N),I=1,M)
      WRITE(6,6080) (AWS(I),I=1,K1)
      WRITE(6,6090) ED
C     COMPUTE CONSTANTS
      G=9.80621
      PI=3.1415927
      PI2=PI *2.0
      RAD=180.0/PI
      DX2=DX*2.0
      DY2=DY*2.0
      EPS=0.01
      DS=DS+A0
      H0=2.828*SQRT(ED)
C     COMPUTE SPECTRUM TRANSFORMATION IN WAVE NUMBER SPACE
C     THIS SUBROUTINE COMPUTES THE BOTTOM SLOPE IN X AND Y
      CALL DEPTH
      DO 20 K=1,K1
      SIGMA=DF*PI*FLOAT(K)
      T=2.0*PI/SIGMA
      HZ=1./T
C     THIS SUBROUTINE COMPUTES CURRENT GRADIENT
      CALL CURENT
C     THIS SUBROUTINE SETS INITIAL VALUES OF WAVE ANGLE AND HEIGHT
      CALL SNELL(THETA,H0,DS)
C     THIS SUBROUTINE CALCULATES WAVE ANGLE
      CALL ANGLE(ITMAX)
```

```
C       THIS SUBROUTINE COMPUTES WAVE HEIGHT
        CALL HEIGHT(ITMAX)
C       COMPUTE ENERGY SPECTRUM
C       TRANSFORM WAVE APPROACHING ANGLE TO DEGREE
        DDW=AWS(K)/ED
        DO 30 I=1,M
        DO 30 J=1,N
        Z(I,J)=(PI-Z(I,J))*180./PI
        E1=(H(I,J)**2)/8.
30      AAW(I,J)=E1*DDW
C       STORE SPECTRAL DENSITY AT SOME STATIONS DESIRED
        DO 40 I=1,IS
        SPDE(K,   I ,I )=AAW(MK(I),NK)
        HERZ(K)=HZ
40      CONTINUE
        WRITE(6,6110)
        WRITE(6,6070) ((Z(I,J),J=1,N),I=1,M)
        WRITE(6,6130)
        WRITE(6,6070) ((H(I,J),J=1,N),I=1,M)
        WRITE(6,6140)
        WRITE(6,6150) ((IB(I,J),J=1,N),I=1,M)
        WRITE(6,6100) HZ
        WRITE(6,6070)((AAW(I,J),J=1,N),I=1,M)
        WRITE(6,6120) HZ
20      CONTINUE
        DO 50 I=1,IS
        WRITE(6,6160) MK(I),NK
        WRITE(6,6170) (HERZ(K),K=1,K1)
        WRITE(6,6180) (SPDE(K,   I ,I ),K=1,K1)
50      CONTINUE
5010    FORMAT(7I5)
5020    FORMAT(7F5.2)
5030    FORMAT(11F5.2)
5040    FORMAT(10F7.4)
6010    FORMAT(/////,1X,'M=',I5,3X,'N=',I5,3X,'K1=',I5,3X,'ITMAX=',I5)
6020    FORMAT(//,1X,'THE DEEP WATER DEPTH=',F8.3)
```

AD-A039 988 DELAWARE UNIV NEWARK DEPT OF CIVIL ENGINEERING F/G 8/3
MEASUREMENTS AND COMPUTATION OF WAVE SPECTRAL TRANSFORMATION AT--ETC(U)
NOV 76 H WANG, W YANG N00014-76-C-0342
UNCLASSIFIED OCEAN ENGINEERING-11 NL

2 OF 2
AD A039988

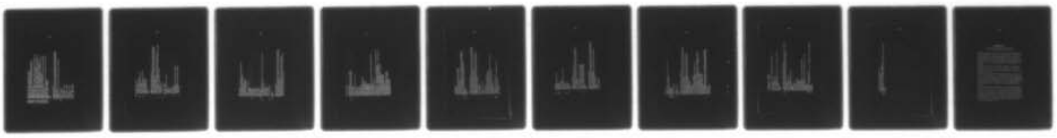

END
DATE FILMED
6-77

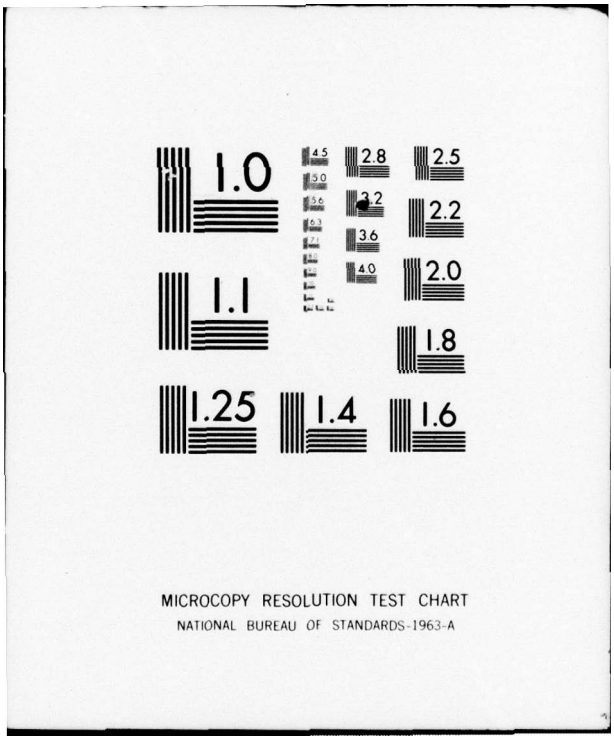
1.0
1.1
1.25
1.4
1.6
1.8
2.0
2.2
2.5
2.8
3.2
3.6
4.0
4.5
5.0
5.6
6.3
MICROCOPY RESOLUTION TEST CHART
NATIONAL BUREAU OF STANDARDS-1963-A

```
6030  FORMAT(//,1X,'DX=',F5.2,3X,'DY=',F5.2)
6040  FORMAT(//,1X,'TIDAL LEVEL=NN+',F6.2)
6050  FORMAT(//,1X,'THE ORIGINAL WAVE DIRECTION IS',F5.2)
6060  FORMAT(//,1X,'THE MATRIX OF WATER DEPTH IN METER')
6070  FORMAT(1X,11F8.3)
6080  FORMAT(//,1X,'ENERGY DENSITY INPUT AT OFFSHORE STATION',1X,
     1'FROM SIGMA=DF*PI/K1 TO DF*PI=',/,10F7.4)
6090  FORMAT(//,1X,'TOTAL WAVE ENERGY AT OFFSHORE STATION=',F7.4)
6100  FORMAT(//,1X,'NEARSHORE SPECTRAL DENSITY AT HZ=',F8.3)
6110  FORMAT(//,1X,'WAVE APPROACHING ANGLE IN DEGREE')
6120  FORMAT(//,1X,'END OF CALCULATION AT HZ=',F8.3,//////////)
6130  FORMAT(//,1X,'WAVE HEIGHT MATRIX')
6140  FORMAT(//,1X,'BREAKING POSITION ("0" MEANS WAVE BREAKING)')
6150  FORMAT(1X,1118)
6160  FORMAT(//,1X,'SPECTRAL DENSITY AT STATION X=',I5,'Y=',I5)
6170  FORMAT(1X,'HERZ=',10F8.3)
6180  FORMAT(1X,'SPDE=',10F8.3)
      STOP
      END

      SUBROUTINE DEPTH
      COMMON D(50,50),U(50,50),V(50,50),Z(50,50),SI(50,50),CO(50,50),
     1H(50,50),CG(50,50),W(50,50),HBREAK(50,50),IB(50,50),DDDX(50,50)
     2,DDDY(50,50)
      COMMON/CON/G,PI,PI2,RAD,EPS,DX,DY,DX2,DY2,T,SIGMA,M,N
      MM1=M-1
  156 DO 157 I=1,MM1
      DO 157 J=2,N
      A=D(I+1,J)
      IF(A.LT.0.0) A=0.0
      B=D(I,J)
      IF(B.LT.0.0) B=0.0
      C=D(I,J)
      IF(C.LT.0.0) C=0.0
      E=D(I,J-1)
      IF(E.LT.0.0) E=0.0
      DDDX(I,J)=(A-B)/DX
```

```
  157 DDDY(I,J)=(C-E)/DY
      DO 100 J=2,N
      DDDX(M,J)=DDDX(MM1,J)
100   DDDY(M,J)=(D(M,J)-D(M,J-1))/DY
      DO 101 I=1,MM1
      DDDX(I,1)=(D(M+1,1)-D(M,1))/DX
101   DDDY(I,1)=DDDY(I,2)
      DDDX(M,1)=DDDX(M-1,1)
      DDDY(M,1)=DDDY(M,2)
      RETURN
      END

      SUBROUTINE SNELL(THETA,HH,DS)
      COMMON D(50,50),U(50,50),V(50,50),Z(50,50),SI(50,50),CO(50,50),
     1H(50,50),CG(50,50),S(50,50),HBREAK(50,50),IB(50,50),DDDX(50,50)
     2,DDDY(50,50),RRK(50,50)
      COMMON/CON/G,PI,PI2,RAD,EPS,DX,DY,DX2,DY2,T,SIGMA,M,N
C     THE FOLLOWING THREE SEGMENTS CALCULATE TANHAA AT OFFSHORE STATION
      CALL WVNUM(DS,0.0,0.0,0.0,0.0,0.0,RK)
      AA=RK*DS
      TANHAA=TANH(AA)
C
      DO 600 J=1,N
   30 DO 600 I=1,M
      IF(D(I,J).GT.0.0) GO TO 33
      ANG=PI
      WVHT=0.0
      SS=0.0
      CC=-1.0
      GO TO 43
   33 CONTINUE
      CALL WVNUM(D(I,J),0.0,0.0,0.0,0.0,0.0,RK)
      AA=RK*D(I,J)
      ANG=ASIN(SIN(THETA)*TANH(AA)/TANHAA)
      ANG=PI-ANG
```

```
      ARG=2.0*AA
      SHOAL=SQRT(1.0/(TANH(AA)*(1.0+ARG/SINH(ARG))))
      REF=SQRT(COS(THETA)/COS(ANG))
      WVHT=HH*SHOAL*REF
      HB=0.12*TANH(AA)*PI2/RK
      IF(WVHT.GT.HB)WVHT=HB
      IN=1
      IF(WVHT.GT.HB) IN=0
      SS=SIN(ANG)
      CC=COS(ANG)
   43 CONTINUE
      H(I,J)=WVHT
      IB(I,J)=IN
      Z(I,J)=ANG
      SI(I,J)=SS
      CO(I,J)=CC
      RRK(I,J)=RK
  600 CONTINUE
C     THE FOLLOWING FIVE SEGMENTS SET INITIAL WAVE HEIGHT TO HO
C     AT OFFSHORE STATION
      IH=(N+1)/2
      HR=HH/H(M,IH)
      DO 10 J=1,N
      DO 10 I=1,M
   10 H(I,J)=HR*H(I,J)
C
  700 RETURN
      END

      SUBROUTINE GROUP
      COMMON D(50,50),U(50,50),V(50,50),Z(50,50),SI(50,50),CO(50,50),
     1H(50,50),CG(50,50),S(50,50),HBREAK(50,50),IB(50,50),DDDX(50,50)
     2,DDDY(50,50),RRK(50,50)
      COMMON/CON/G,PI,PI2,RAD,EPS,DX,DY,DX2,DY2,T,SIGMA,M,N
      COMMON/UV/ DUDX(50,50),DUDY(50,50),DVDX(50,50),DVDY(50,50)
      DIMENSION DTDX(50,50),DTDY(50,50)
```

```
      DO 400 I=2,M-1
      DO 400 J=2,N-1
      DTDX(I,J)=(Z(I+1,J)-Z(I-1,J))/DX2
400   DTDY(I,J)=(Z(I,J+1)-Z(I,J-1))/DY2
      DO 500 I=1,M
      DO 500 J=1,N
      IF(D(I,J).LE.0.0) GO TO 500
      DEP=D(I,J)
      COSI=CO(I,J)
      SINI=SI(I,J)
      RK=RRK(I,J)
      TA=TANH(RK*DEP)
      HBREAK(I,J)=0.12*PI2*TA/RK
      COSH1=COSH(RK*DEP)
      SECHSQ=1.0/(COSH1**2)
      ARG2=2.0*RK*DEP
      SINH2=SINH(ARG2)
      COSH2=COSH(ARG2)
      SINHSQ=SINH2**2
      E=U(I,J)*COSI+V(I,J)*SINI+0.5*SIGMA*(1.0+ARG2/SINH2)/RK
      C=SQRT(G*TA/RK)
      FF=0.5*(1.0+ARG2/SINH2)
      CG(I,J)=FF*C
      DKDX=RK*((U(I,J)*SINI-V(I,J)*COSI)*DTDX(I,J)-(COSI*DUDX(I,J)+
     1SINI*DVDX(I,J))-SIGMA*DDDX(I,J)/SINH2)/E
      DKDY=RK*((U(I,J)*SINI-V(I,J)*COSI)*DTDY(I,J) -(COSI*DUDY(I,J)
     1 +SINI*DVDY(I,J))-SIGMA*DDDY(I,J)/SINH2)/E
      P=C*(SINH2-ARG2*COSH2)/SINHSQ
      DKDDX=RK*DDDX(I,J)+DEP*DKDX
      DKDDY=RK*DDDY(I,J)+DEP*DKDY
      Q=0.5*G/(C*RK**2)
      DCDX=Q*(RK*SECHSQ*DKDDX-TA*DKDX)
      DCDY=Q*(RK*SECHSQ*DKDDY-TA*DKDY)
      DCGDX=P*DKDDX+FF*DCDX
      DCGDY=P*DKDDY+FF*DCDY
```

```
      SS2=SINI**2
      CC2=COSI**2
      SIGXX=(2.0*FF-0.5)*CC2+(FF-0.5)*SS2
      SIGYY=(2.0*FF-0.5)*SS2+(FF-0.5)*CC2
      TAUXY=FF*SINI*COSI
      S(I,J)=CG(I,J)*(SINI*DTDX(I,J)-COSI*DTDY(I,J))-(DUDX(I,J)+
     1DVDY(I,J))-(COSI*DCGDX+SINI*DCGDY)-(SIGXX*DUDX(I,J)+TAUXY*
     2DUDY(I,J)+TAUXY*DVDX(I,J)+SIGYY*DVDY(I,J))
500   CONTINUE
      RETURN
      END

      SUBROUTINE HEIGHT(ITMAX)
      COMMON D(50,50),U(50,50),V(50,50),Z(50,50),SI(50,50),CO(50,50),
     1H(50,50),CG(50,50),S(50,50),HBREAK(50,50),IB(50,50),DDDX(50,50)
     2,DDDY(50,50),RRK(50,50),C(50,50)
      COMMON/CON/G,PI,PI2,RAD,EPS,DX,DY,DX2,DY2,T,SIGMA,M,N
      COMMON/UV/DUDX(50,50),DUDY(50,50),DVDX(50,50),DVDY(50,50)
C     COMPUTE VALUES OF S(I,J)
      CALL GROUP
      DO 10 II=1,M-1
      I=M-II
      DO 20 IT=1,ITMAX
      IFLAG=1
      DO 30 J=2,N
      IF(D(I,J).LE.0.0) GO TO 30
      CC1=(V(I,J)+CG(I,J)*SI(I,J))/DY
      CC2=(U(I,J)+CG(I,J)*CO(I,J))/DX
      HNEW=(CC1*H(I,J-1)-CC2*H(I+1,J))/(CC1-CC2-S(I,J)/2.0)
      IF(HNEW.LE.HBREAK(I,J)) GO TO 850
      HNEW=HBREAK(I,J)
      GO TO 860
850   IF(HNEW.LT.0.0) HNEW=0.0
860   IF(ABS(HNEW-H(I,J)).GT.(EPS*ABS(HNEW))) IFL=0
      IF(IFL.EQ.0) IFLAG=0
      H(I,J)=HNEW
```

```
30    CONTINUE
      IF(IFLAG.EQ.1) GO TO 10
20    CONTINUE
10    CONTINUE
      DO 40 I=1,M
      DO 40 J=1,N
      IF(H(I,J)-HBREAK(I,J)) 2,3,3
2     IB(I,J)=1
      GO TO 40
3     IB(I,J)=0
40    CONTINUE
      RETURN
      END

      SUBROUTINE CURENT
      COMMON D(50,50),U(50,50),V(50,50)
      COMMON/UV/DUDX(50,50),DUDY(50,50),DVDX(50,50),DVDY(50,50)
      COMMON/CON/G,PI,PI2,RAD,EPS,DX,DY,DX2,DY2,T,SIGMA,M,N
      DO 20 I=2,M-1
      DO 20 J=2,N-1
      DUDX(I,J)=(U(I+1,J)-U(I-1,J))/DX2
      DUDY(I,J)=(U(I+1,J)-U(I-1,J))/DY2
      DVDX(I,J)=(V(I+1,J)-V(I-1,J))/DX2
20    DVDY(I,J)=(V(I,J+1)-V(I,J-1))/DY2
      RETURN
      END

      SUBROUTINE ANGLE(ITMAX)
      COMMON D(50,50),U(50,50),V(50,50),Z(50,50),SI(50,50),CO(50,50),
     1H(50,50),CG(50,50),S(50,50),HBREAK(50,50),IB(50,50),DDDX(50,50)
     2,DDDY(50,50),RRK(50,50)
      COMMON/CON/G,PI,PI2,RAD,EPS,DX,DY,DX2,DY2,T,SIGMA,M,N
      DO 200 IT=1,ITMAX
      IFLAG=1
      DO 210 J=2,N
      DO 211 II=2,M-1
```

```
      I=M-II+1
      IF(D(I,J).LE.0.0.OR.D(I-1,J).LE.0.0) GO TO 211
      CALL NEWANG(I,J,IFLAG,2)
  211 CONTINUE
  210 CONTINUE
  200 CONTINUE
      DO 300 I=2,M-1

  300 Z(I,1)=Z(I,2)
      RETURN
      END

      SUBROUTINE NEWANG(I,J,IFLAG,IM)
      COMMON D(50,50),U(50,50),V(50,50),Z(50,50),SI(50,50),CO(50,50),
     1H(50,50),CG(50,50),S(50,50),HBREAK(50,50),IB(50,50),DDDX(50,50)
     2,DDDY(50,50),RRK(50,50)
      COMMON/CON/G,PI,PI2,RAD,EPS,DX,DY,DX2,DY2,T,SIGMA,M,N
      COMMON/UV/DUDX(50,50),DUDY(50,50),DVDX(50,50),DVDY(50,50)
      ARG2=2.0*RRK(I,J)*D(I,J)
      SINH2=SINH(ARG2)
      COSI=CO(I,J)
      SINI=SI(I,J)
      F=U(I,J)*COSI+V(I,J)*SINI
      FF=F+0.5*(1.0+ARG2/SINH2)*(SIGMA/RRK(I,J)-F)
      F1=(SIGMA-RRK(I,J)*F)/SINH2
      DKDY=(-(COSI*DUDY(I,J)+SINI*DVDY(I,J))-(F1*DDDY(I,J)))/FF
      DKDX=(-(COSI*DUDX(I,J)+SINI*DVDX(I,J))-(F1*DDDX(I,J)))/FF
      FACI=U(I,J)*SINI-V(I,J)*COSI
      DEN1=(SINI-COSI*FACI/FF)/DY
      DEN2=(COSI+SINI*FACI/FF)/DX
      DEN=DEN1-DEN2
      ZNEW=(COSI*DKDY-SINI*DKDX+Z(I,J-1)*DEN1-Z(I+1,J)*DEN2)/DEN
C     THE FOLLOWING FIVE SEGMENTS SET OVERFLOW PROTECTION FOR ZNEW
      ZA=DY/DX
      ZC=ATAN(ZA)
      ZD=ZC-0.05+PI
```

```
      IF(ZNEW.GT.ZD) ZNEW=ZD
      IF(ZNEW.LE.0.) ZNEW=ZD
C
      IF(ABS(ZNEW-Z(I,J)).GT.(EPS*ABS(ZNEW))) IFLAG=0
      Z(I,J)=ZNEW
      CO(I,J)=COS(Z(I,J))
      SI(I,J)=SIN(Z(I,J))
      CALL WVNUM (D(I,J),CO(I,J),SI(I,J),U(I,J),V(I,J),RK)
      RRK(I,J)=RK
       RETURN
      END

       SUBROUTINE WVNUM(D,COSI,SINI,U,V,RK)
C SUBROUTINE COMPUTES THE WAVE NUMBER INCLUDING WAVE-CURRENT INTERATION
      COMMON/CON/G,PI,PI2,RAD,EPS,DX,DY,DX2,DY2,T,SIGMA,M,N
      EPSK=0.0005
      RK=PI2/(T*SQRT(G*D))
      DO 100 I=1,50
      A=SIGMA-U*RK*COSI-V*RK*SINI
      A2=A**2
      ARG=RK*D
      F1=EXP(ARG)
      F2=1.0/F1
      SECH=2.0/(F1+F2)
      SECH2=SECH*SECH
      TT=TANH (ARG)
      FK=G*RK*TT-A2
      FFK=G*(ARG*SECH2+TT)+2.0*(U*COSI+V*SINI)*A
      RKNEW=RK-FK/FFK
      IF(ABS(RKNEW-RK).LE.(ABS(EPSK*RKNEW))) GO TO 110
      RK=RKNEW
  100 CONTINUE
      WRITE(6,101) I,RK,T,D,U,V
  101 FORMAT('  ITERATION FOR K FAILED TO CONVERGE AFTER',I6,3X,5F10.4)
      RETURN
  110 RK=RKNEW
```

```
      SIGMA=SIGMA-U*RK*COSI-V*RK*SINI
      IF(RK.GT.0.0) GO TO 120
      WRITE(6,130) D,COSI,SINI,U,V,RK,SIGMA
  130 FORMAT(10X,'RK IS NEGATIVE--OUTPUT D,COSI,SINI,U,V,RK,A'/,7E12.4)
  120 RETURN
      END
```

Zusammenfassung

Messungen und Berechnungen der Veränderung
von Wellenspektren vor der Insel Sylt

Im Küstenvorfeld der Insel Sylt, rd. 900 m seewärts, wurden Wellenspektren gemessen. Die im Mai 1976 für die Dauer von zwei Wochen betriebene Meßkette umfaßte sieben Stationen. Die Ergebnisse der Naturmessungen wurden nach der Auswertung mit einem von den Verfassern für dieses Projekt vorher entwickelten numerischen Berechnungsansatz für die Energieumwandlung in Flachwassergebieten verglichen.

Die Werte der numerischen Berechnung zeigten eine gute Übereinstimmung mit den Daten aus der Natur im Bereich der unteren und mittleren Frequenzen; im Bereich hoher Frequenzen war die Übereinstimmung weniger gut.

Ausgehend von den bekannten Stabilitätskriterien für Wellen wurde eine Gleichgewichtsfunktion der spektralen Energiedichte für Bereiche mit beschränkter Wassertiefe entwickelt, die für das gesamte Spektrum gute Übereinstimmung hinsichtlich der Spektraldichte zeigt. Die Vergleiche mit den Naturmessungen fallen ebenfalls gut aus, es bedarf jedoch weiterer Messungen für eine allgemeingültige Bestätigung.

Aus der Verbindung von Meßergebnissen und theoretischen Berechnungen konnten Aussagen über das Wellenklima des Untersuchungsgebietes vor Sylt gemacht werden. Es wurde gezeigt, daß das küstenparallele Riff eine Doppelfunktion als Energie umwandelnde und Energie konzentrierende morphologische Formation hat. Weiterhin konnte abgeleitet werden, daß Wellen aus dem NW- Quadranten den größten Einfluß auf die Entstehung von Küstenlängsströmungen und damit auf den Küstenlängstransport haben.